Department of Precision and Microsystems Engineering

Designing a Visual Effect to Replace the Needle Indicator of an Advanced Mechanical Stopwatch Function

Bram Wielaard

Report No. : 2023.035
Coach : Alden Yellowhorse
Professor : Hans Goosen
Specialisation : High-Tech Engineering
Type of report : Design Report
Date : 13^{th} June 2023

TU Delft

DELFT UNIVERSITY OF TECHNOLOGY

THESIS

Designing a Visual Effect to Replace the Needle Indicator of an Advanced Mechanical Stopwatch Function

Bram Wielaard

The luxury watchmaking industry responds neither to needs nor to problems. [...] we actually create new “problems” [...] We literally add “complications” to our customers’ lives. [1]

~

Georges A. Kern
CEO of Breitling

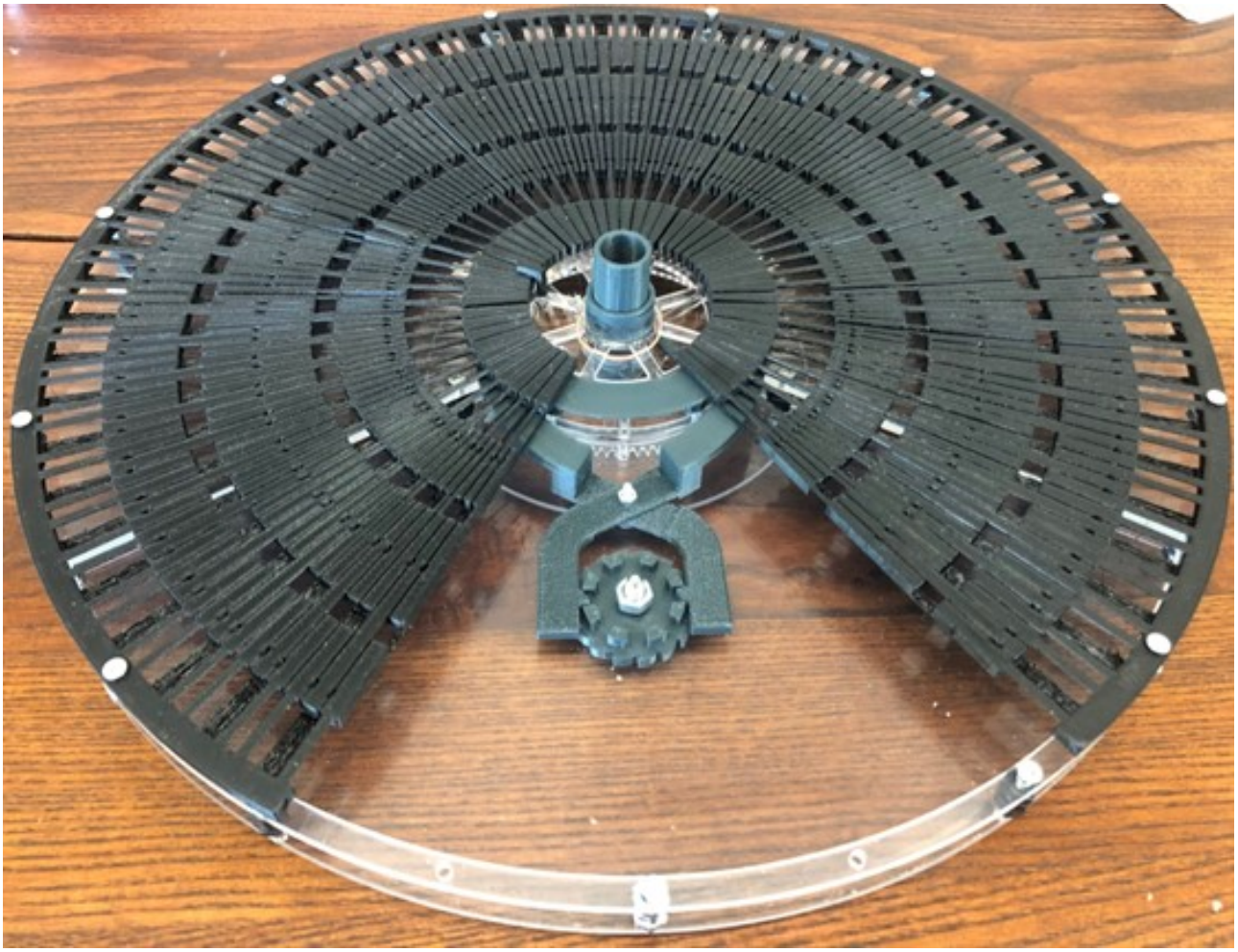

Abstract

This thesis describes the process of designing a visual effect to replace the needle indicator of a rattrapante complication. The mechanisms of the chronograph and rattrapante are explained as well as the importance of aesthetics in the luxury watchmaking industry. After establishing a method to determine a feasible design, the criteria that need to be fulfilled for the final design are quantified. Extra attention is given to: the minimum part size with respect to human visibility; assessing the aesthetic value of different visual effects based on a survey; and quantifying the maximum rotational inertia by means of a friction study. From the aesthetically pleasing ideas from the survey feasible concepts are generated as well as weighted with respect to each other. The best concept is turned into a working mechanism by establishing a production method and calculating stresses in compliant flexures. A torsion hinge that can be produced from a double-BOX-layered silicon wafer is also designed. The actuation by a discrete vertical clutch gripper is designed as well as the extra parts needed for a fully functioning mechanism that fits the design space. As a result, a demonstrator at scale 15:1 is build to show the working mechanisms of the design as well as the visual effect itself. It concludes with a successful mechanism which probably also has relevance in other watches.

Keywords: Horology, Rattrapante, Aesthetics, Visual Effect, Needle Indicator, Compliant Flexure Stress, Discrete Vertical Clutch Gripper, Double-BOX-layered Silicon Wafer.

Contents

1 Introduction

Before starting with the main theme of this thesis, designing a visual time imprint, I would like to introduce the reader the thoughts behind this design, the rattrapante and aesthetic design in the watchmaking world. If one is unfamiliar with mechanical watches, it is recommended to check out [2]. This site has a step-by-step explanation of the parts of a mechanical watch and how they are connected to each other.

Mechanical watches have been complicated in many different ways since their first occurrence in 15^{th} century [3, pp.128]. Automatic winding for example improves the ease of use of the watch by removing the need to manually wind the watch every few days [4]. Other complications, like the tourbillon or triaxial tourbillon, aim to improve the accuracy of the watch by canceling out the influence of gravity over time [5, 6]. However, most complications add an extra function to the watch: like world clocks to show the time in different timezones [7]; datographs to show the current day, date or even year [8]; moonphase dials to track the current phase of the moon [9]; chronographs to time the duration of an event [10]; or rattrapantes, which allow to take multiple measurements of the same event as an addition to a chronograph [11]. And lastly, some complications add functionality for very specific groups of people, like minute repeaters to ring the time for blind people [12] or zero-reset functions to allow for great synchronization of multiple watches in, for example, military uses [13].

Even though mechanical watches could have become obsolete due to quartz watches and digital clocks, which are way more accurate [14–16], mechanical watches have nested themselves as a niche luxury product. They allow people to show their social status; to express themselves; and their owner to focus on the inessential [1]. Also, mechanical watches never lost their mechanical intricacy which gives people a feeling of inventiveness a superiority over past times [17].

1.1 Design Objective

One thing almost all watches have in common is a needle indicator. Needle indicators are present in everyday life for humans and are used for decision making in many situations. For example, one will stop at the next gas station based on their fuel tank indicator, someone will start running for his train based on their watch indicator and a pilot will adjust its landing speed based on a needle indicator. One can argue that the accuracy of such a needle indicator is disputable. Since a needle indicator floats above the dial, looking at it from a different angle will change the readout result and data collected by [18] and [19] show that the readout is not error free. One can image the catastrophic results if the readout by the pilot of its instrument is not accurate.

Watches can feature many needles. Next to the standard hour, minute and seconds hands, datograph, chronograph and rattrapante complications also add extra needles to a watch. This thesis aims to change the needle indicator for the rattrapante complication. Due to the nature of the rattrapante hand, which becomes stationary on demand, one could design a variation that creates a visual imprint of the current time.

The luxury mechanical watchmaking industry is a heavily patented one, so one needs to check if this idea is new. By conducting a patent search one can show that that creating a variation for the needle indicator is not a new idea. Some returning themes in these patents can be categorized in the following themes: digital displays [20–23], aperture views [9, 24, 25], retrograde indicators [26, 27], linear displays [28–30], radial effects [31], flexible paths [32–34], revolving 3D shapes [35–37], rotating discs [38, 39] and non-concentric indicators [40, 41].

This patent search did however, not find any variations of the needle indicator in a rattrapante mechanism. This generates a design objective for this thesis: ”design a complication that replaces the needle indicator of a rattrapante mechanism with a visual effect”.

1.2 The Rattrapante

One might currently be wondering what a rattrapante complication is, apart from the ’it allows to take multiple measurements of the same event’ and how it works. Before the rattrapante can be explained, one first needs to know about the chronograph.

The chronograph would in layman’s terms be called a stopwatch. The chronograph complication features an extra needle, most of the time in red, which is stationary at the 12 o’clock position. By pressing a button on the side of the watchcase one can start the chronograph needle. The chronograph needle will connect to the main geartrain of the watch and start its own time measurement. When stopped by pressing the same button again, the chronograph will disconnect from the geartrain and one can read out the time passed since the start of this run. A second button on the watchcase will reset the chronograph needle to the 12 o’clock position, allowing for multiple subsequent measurements.

The mechanism behind these steps is more difficult than the explanation above makes it seem to be, so some sources for further reading and images showing their working are referenced. The start-stop button is directly connected to a column wheel [42, pp.236] and [43], which it rotates. This column wheel connects or disconnects, by means of a vertical [44] or horizontal clutch [45], an ’intermediary chronograph wheel’ to the gear train. It moves this gear to be connected to the seconds gear of the watch. The seconds gear then directly drives the chronograph hand. When the reset button is pressed a ’hammer’ is released. This hammer strikes a cam, which is on the chronograph axis, to force it back into the 12 o’clock position. To ensure this position is deterministic this cam is heart shaped, which will always want to rotate in such a way that the belly of the heart comes into connection with the hammer. [46] shows this heart shaped cam and how the hammer strikes it. The heart shape is also present in the rattrapante mechanism and will be analyzed in Section 3.3.4 more in depth.

A rattrapante complication features a second needle, the rattrapante hand. This rattrapante hand is located directly underneath the chronograph hand, and when the chronograph is

started it will travel in unison, and thus out of sight of its user. The extra complication is that the rattrapante hand can be stopped separately with the use of a third button.

Figure 1 shows how a stopped rattrapante looks like. With the rattrapante hand (2.2) stationary and chronograph hand (8.2) still running. The chronograph hand can later be stopped by using the very first button. This allows the user to, for example, time two horses running on the same track and measuring their respective finishing times ór time the lap times of a single runner running multiple laps. If the runner passes the finish, stop the rattrapante, write down the time, and release the rattrapante. Releasing the rattrapante needle will make it catch up ('rattraper' translates to 'to catch up' from french) to to where the chronograph needle currently is and it will start running in unison with it as if it was never stopped. This can be repeated over any amount of laps this runner will make. This video [48] is a nice demonstration of how those steps look if one uses a rattrapante.

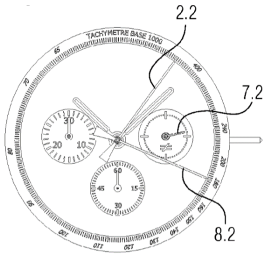

Figure 1: An illustration of a 'split-time' on a rattrapante [47].

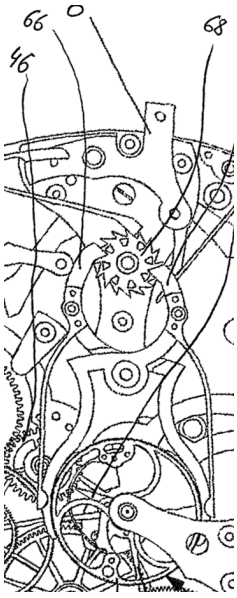

Figure 2: Illustration of the gripping mechanism to stop the rattrapante hand [49].

The rattrapante mechanism is quite difficult, thus some images are provided to shows how this mechanism works. The third button is connected to a second column wheel (68). This column wheel activates a gripper (66). This gripper is the mechanism that allows the rattrapante gear (68) to be stopped and is shown in Figure 2. It grabs the rattrapante wheel, which has the shape of a gear but is not driven by the gear train, its function is simply to be grabbed and stopped. The rattrapante needle is driven by a spring (34) that is in connection with a second heart shaped cam (32) on the chronograph axis as shown in Figure 3a. This spring makes sure the rattrapante and chronograph are not rigidly connected, and thus allows, when stopped, the spring to follow the shape of the heart (that will keep rotating with the chronograph), as shown in Figure 3b. If the rattrapante is released, this spring will exert a force on the rattrapante and make sure the rattrapante is pushed to the belly of the heart. If calibrated correctly, this will make the chronograph and rattrapante hand line up once again.

Before continuing, I want to highlight the uniqueness of a rattrapante complication. The rattrapante complication was first designed in 1838 , however, the first rattrapante was only build

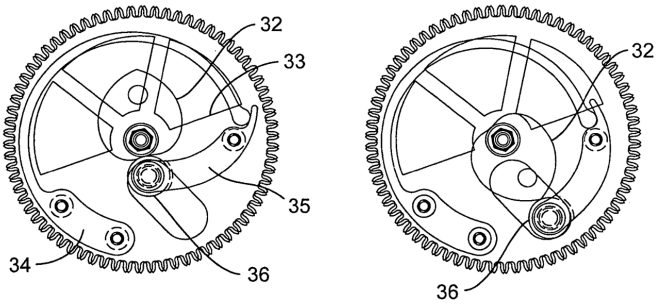

Figure 3: Illustrations of a rattrapante hand a) synchronized and b) not synchronized with the second-hand of the chronograph [50].

about a hundred years later in 1912 [51]. This highlights the difficulty in assembling such a system, even for master watchmakers. Also, currently, about 50 to a 100 watches featuring a rattrapante are produced a year, with prices around €60,000 not uncommon, which highlights the luxury and rarity of such a watch [52].

1.3 Aesthetics

Knowing the price tag and uniqueness of a rattrapante it is safe to assume that the customers want something they find 'pretty'. G. Kern states in [1] that in watchmaking art and product design come together: watches need a high precision and finesse to keep the time, but their design is guided by art and aesthetics. Watchmaking and aesthetics thus come hand in hand. However, aesthetics is a difficult term to quantify [53]. The Standford University encyclopedia [54] defines aesthetics as: "'aesthetic' has come to designate, among other things, a kind of object, a kind of judgment, a kind of attitude, a kind of experience, and a kind of value." The encyclopedia is however skeptical on the use of the term 'aesthetic' as basis for an meaningful theoretical argument. Also, within aesthetics there are 2 main subcategories [55]: a broad one focused on "beauty, aesthetic pleasure, and preference" and a narrow one focused on the "research on the perception, evaluation, and creation of art."

Let's assume that for this subject aesthetics has a close relation to art, and is a response to an object that provokes an emotion and can indicate value. According to [56] the 'aesthetic response' is rapid, involuntary, two-sided (either positive/pretty or negative/ugly) and cannot be changed easily after that initial assessment. According to [57] the aesthetic response is mainly based on the shape, the color and the material of the product someone is looking at it.

Since the aesthetic response is an emotion it differs per person. According to [58] it will be influenced by the person itself (biological) and their cultural upbringing. They even state that humans exhibit false and true aesthetic emotions, implying that a person might not always be aware of their own aesthetic response. As a consequence asking people about their aesthetic

emotions does not always yield a truthful, and thus accurate, answer. Simply because they do not know themselves.

In summary, aesthetics is difficult to objectively quantify, nor is the person always aware of their own response, nor can a cultural and biological element be factored out [59]. This brings out a crucial question: how does one design a product that creates a positive aesthetic response? Literature provides some generic insights: according to [60] the aesthetic value will suffer if it is not clear from the start what the functionality of the product is; [61] concludes that creativity in general has a positive influence on aesthetics; and [62] argues that humans give a high aesthetic value to natural patterns.

Aesthetics in relation to watchmaking seem to be mainly related to observing the movement of the watch [63]. And to come back to Georges Kern [1]: he states that decisions on aesthetics within luxury watchmaking companies are sometimes undemocratic. The manager might decide what their preference is. Because for a luxury brand there is "nothing so spineless as "A majority of executive committee members have voted in favor of launching this product" or "This finding has been tested by market research."

When designing for an aesthetically pleasing product, the functionality should be clear for the customer, it should be a creative design and should ideally show parts of the watch movement. However, it should not be decided upon simply by the designer, since that is just one person with their own biological and cultural taste. Also, according to [64] designers and customers understand products differently, which means that the designer itself cannot decide upon a clear functionality. For this study a method should be produced to establish an independent quantification of aesthetic value. The selected method is detailed in Section 2.

2 Method

This section describes the method that aimed to deliver a feasible and valuable end design. All the criteria this design should adhere to were be quantified. Most criteria were straightforward, however some were not and needed some extra steps to be meaningful. All the criteria were researched and quantified in Section 3. The visual effects that were ranked the highest in the aesthetic survey in Section 3.2 were turned into concepts in Section 4. Different mechanisms were conceptualized to generate the desired effect and based on the criteria it was checked if these mechanisms were feasible. The feasible concepts were weighted using the weighted criteria method to determine which concept would be used as the final design in Section 5.

A schematic of these design steps is shown in Figure 4. Which shows that, out of all the possible visual effects, a set of visual effects is created. Since achieving completeness in a creative design space is simply not possible, this set will not span the entirety of all effects. From this set, the aesthetically pleasing idea were selected by means of the survey, and for those effects feasible mechanisms were be generated. The final design

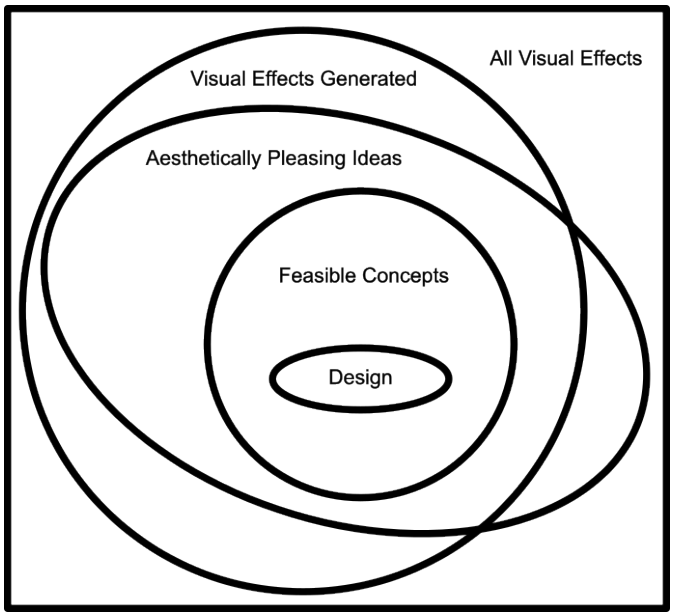

Figure 4: A schematic Venn Diagram of how the design space converge to the final design.

was chosen from one of these feasible, aesthetically pleasing concepts.

Section 6 describes the generation of the final design, and all things that come with it to achieve a working demonstrator. This demonstrator, in Section 7, was build on scale (due to the fact that I am not a master watchmaker and the rattrapante is hard to assemble) and Section 8 analyzes the end results and its relevance.

3 Criteria

This section includes the overview of the criteria that needed to be satisfied in order to produce a 'good' design. Following the established method in Section 2, it quantifies and lists all the different criteria. Since some criteria were not straightforward some criteria are explored more in-depth.

In Section 3.1 the minimum parts size with respect to human sight was researched followed by Section 3.2 where the aesthetic value of different visual effects was assessed. In Section 3.3 a model was build to convert the given torque criterion into rotational inertia and in Section 3.4 an elaboration for all other criteria is given. In Section 3.5 a complete list of all the quantified criteria as well as some wishes was compiled.

3.1 Visibility

To make sure that customers can see, and thus use, the designed mechanism it should be clearly visible. The visibility of an object depends on 2 main things: the minimum size a human eye can see, and the contrast of the object with respect to the surroundings [65].

The minimum size a human eye can distinguish differs per person and based on their acuity and the viewing distance. Normal vision is indicated by 20/20 feet acuity (or 6/6 meters) and minimum visible size is calculated using Equation 1, [66],

$$\frac{X}{2} = d\,\frac{tan(\theta)}{2}, \tag{1}$$

where θ is defined by the acuity and is 1/60 degrees for 20/20 acuity, d is the viewing distance and X is the size of the object. According to [67], the viewing distance d for wristwatches is between 305 and 600 mm. This means that the minimum visible size lies between 90 and 175 µm.

However, our eyes also need contrast to distinguish objects. [68] states that "any visual task can be made invisible by progressive reduction of its contrast down to a threshold value." [69] presents a formula for the "luminance contrast" which is based on the difference in luminance of the object and its surroundings. They consistently show that below a certain contrast level distinguishability decreases quickly. This means that the system needs enough contrast, which is supported by the fact that a lot of watches use black or red hands on a white dial.

So, the design should not have parts smaller than 90 µm and should exhibit some contrast with its surroundings.

3.2 Aesthetic Evaluation

As described in the method, this section is dedicated to establish a list of aesthetically pleasing ideas. By creating as many different visual effects as possible and ranking their aesthetic value based on a survey, this section identified the highest scoring ideas as assessed them as aesthetically pleasing.

First in Section 3.2.1 ideas for possible visual effects were be generated in a standard format. In Section 3.2.2 a survey was conducted and in Section 3.2.3 a list of aesthetically pleasing visual effects is presented based on the results of the survey.

3.2.1 Idea Generation

As described in Section 2 and schematically shown in Figure 4 the ideas will try to cover the span of all possible visual effects as much as possible. To achieve this, to not limit creativity and inspiration, very little attention was paid to mechanical feasibility during this idea generation. However, ideas using lamps were omitted due to the absence of electricity in a mechanical watch.

All effects were created in the same format that consists of three top view watch cases: the first is in a neutral phase, the second shows the rattrapante stopped at 10 seconds whilst the chronograph hand moved to 50 seconds, and the third watch case, in the same time position, was included to allow for a variation, range extension (more than 60 seconds), accuracy improvement or clarification of the idea. The third was thus not utilized for all effects. This format is shown in Figure 5 for a standard rattrapante with 2 needles and no visual effect.

Most effects were created with an accuracy of 12 steps (5 second precision) and in grey-scale to remove the influence of color preference of survey participants. The effects have a name by which they are referred to, most of them based on a description of the visual effect, some based on the mechanical principle and others on the everyday 'object' that inspired it. The 30 visual effects generated are all shown in Appendix A.

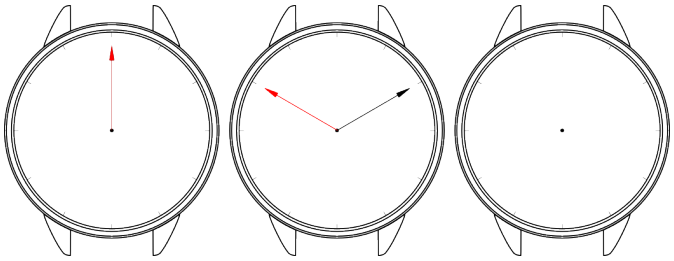

Figure 5: The template of the ideas for visual effects. From L to R: a rattrapante and chronograph currently not in use; a rattrapante stopped at 10s and a chronograh stopped at 50s; an empty watchcase for a variation or clarification.

3.2.2 Survey Execution

As stated these ideas were evaluated by a survey. The group consisted of 19 participants and was slightly dominated by male engineers. To counter this, different weighted scores were compared. This survey was be used as a guideline, and thus not only the top idea was considered (as will become clear in Section 3.2.3).

The survey was conducted in the following manner: by printing two effects on a page in no particular order and sticking them on a wall of a meeting room in no particular order the effects were presented to the survey participants. The closed door meeting room guaranteed no 'outside' influence on opinion from other participants. The participants were invited in in no particular order (mainly driven by presence over a couple of days) and shortly introduced to the rattrapante (if not familiar already) and the goal of the project (replacing the rattrapante hand) and the format of the 3 watch cases.

After this introduction the people were given the time and space, physically and mentally (by me stepping backward 2 or 3 meters), to take a look at the effects presented. They were asked to give their opinion on the presented effects: which ones are aesthetically pleasing and which are not. As explained in Section 1.3 the aesthetic response is rapid [56]. There was no need to let people rank all the effects from 1 to 30, but they were simple asked to select their top and bottom few. The ratings people gave were noted as a plus or a minus on that particular effect, and sometimes some small notes were added. f.e. if the idea was bad because it was unclear. Comments like those were worked out and are shown in Appendix B. To analyze the data gathered all the votes of people were represented as numbers in a table. For every effect they commented on a +1 or -1 was added in their respective row.

The respondents were sorted into multiple categories:

- Invested: that are either close to and/or have specific benefit if this study delivers a successful result.

- Business: Individuals that are not engineers.
- Research and Design: Individuals with an engineering background.
- Lab and Intern: Individuals that are not (yet) engineers nor business.

The people in the invested group might belong in another subgroup as well, but they are removed there to be represented only once.

From the data three different scores were constructed.

- Neutral: Each vote counts once over the entire table. A ratio for this score is included, It divides the score by the amount of votes cast. This shows if people were unanimous in their opinion of each effect.
- M/F: The male to female ratio is set to one (each vote of a woman weighs more than that of a man) since the watch is unisex, this might influence the results.
- Weighted: The Invested people have a double weight in this score and the Head of Marketing has weight factor 4 (since their job is aesthetics). Their opinion is allowed to matter more since luxury product design is sometimes undemocratic [1]. Also, to slightly account for the difference between an engineering viewpoint and a 'business' viewpoint the business group is also counted double to compensate for their smaller sample size.

3.2.3 Survey Results

Using the survey results Table 1 was generated. The effects are sorted on the weighted score in this table, but as one can see, the order of the effects when sorted by different scores varies only slightly. From the table it was concluded that there definitely were some aesthetically good and bad ideas: the 'Sine on Circle', the 'Ferro Tube', the 'Origami Fan', the 'Mechanical Mirrors' and the 'Ferrofluid' ideas were assessed as aesthetically good ideas.

Based on the feedback and notes of participants, which can be read in Appendix B, the following three ranked effects were analyzed: The 'spirals' has a low ratio. The fact that it is not very clear was a frequent comment but will not solve the fact that a lot of people did not like it either way. It was thus be discarded.

The 'Magnetic Field' was well received but the small needle size makes it hard to read according to some. The 'Aiming Diamonds' is more clear due to the larger needles, however the width of the diamonds makes it less aesthetically pleasing. Reviewing the basis of these effects one can conclude they are quite similar. Both aim 'needles' that are distributed over the entire dial at a point in space, the first by following magnetic field lines, the second by following gradients. By combining the participants comments they can both easily be improved: needles that scale with the radius and do not have the shape of a diamond. Thus, these two effects were both be taken as aesthetically pleasing ideas.

This means that there are seven effects now deemed feasible for concept generation. They are:

- Sine on circle
- Ferro Tube
- Origami Fan
- Mechanical Mirrors
- Ferrofluid
- Magnetic Field
- Aiming Diamonds

The Figures are shown in their respective sections where mechanisms will be examined for possible concepts 4. The survey results delivered a clear quantification of the 'aesthetic value' criterion.

Table 1: The results of the aesthetic survey in tabular form and sorted by the 'Weighted' score.

Ratio	M/F Score	Weighted Score	Effect Name	Invested	Business	R&D	Lab&Intern
1.000	12.6	16	Sine on circle	5	1	3	1
0.778	11.4	15	Ferro Tube	5	2	1	0
1.000	10.6	13	Origami Fan	4	0	3	2
0.750	6.8	11	Mech Mirror	4	0	2	1
0.750	6.8	10	Ferrofluid	3	0	2	2
0.500	7.6	9	Spirals	4	0	1	0
0.455	6.8	8	Magnetic Field	2	0	2	2
0.600	6	7	Aiming Diamonds	1	0	3	2
1.000	4	6	Revolving Balls	2	0	2	0
1.000	5	6	Web Moving	1	0	3	1
1.000	2	4	Outer Edge Indicator	1	1	0	0
0.500	2	3	Noncentric	1	0	0	1
0.429	2	3	Revolving pyramids	1	0	0	1
0.000	3.6	2	Hex Sideway	2	-1	1	-1
0.333	1	1	Cat eye	0	0	1	0
0.000	0	1	Ferro Loose	0	1	-1	0
0.333	2.8	1	Roof Tiles	-1	1	1	0
-0.143	-1	-1	Hex updown	0	0	0	-1
-1.000	-3	-4	Radial Engine	-1	0	-1	-1
0.000	-0.8	-5	Digital aperture	-4	0	3	0
-0.600	-8.4	-6	Golden Ratio	-2	0	-2	0
-1.000	-7.8	-7	Flipping Triangles	-1	0	-3	-2
-0.714	-6.8	-9	Origami Sphere	-2	-1	-3	0
-0.714	-5	-9	Bending Datawaves	-3	0	-1	-2
-1.000	-7.6	-9	Opening Circle	-4	0	-1	0
-0.400	-8.4	-11	Digital	-5	-1	-1	2
-0.833	-12.6	-11	Radial Effect	-1	-1	-5	-2
-0.750	-9.6	-11	Mandela	-4	0	-2	-1
-1.000	-13.6	-13	Triangles Rotate	-2	-1	-5	-2

3.3 Friction Study

This section focuses on converting the torque criterion to a more straightforward variable: rotational inertia. This was done using a Matlab® Simulink model, that represents a reference watch, with which data could be gathered for an inertia criterion.

First, an introduction on how torque and friction influence the runtime of the watch is given in Section 3.3.1, it also describes why a conversion to inertia was chosen as a goal for this friction study. After that a base model that resembles and runs like the reference watch was created in Section 3.3.2. Section 3.3.3 describes how the heart shape was defined and in Section 3.3.4 a vertical clutch chronograph as well as a rattrapante were added to the system. The complete model was then analyzed to check if the 8.25 mNm is a reasonable criterion in Section 3.3.5 and used to find the limits of the rotational inertia of the rattrapante in 3.3.6.

3.3.1 Friction Influence

When adding a rattrapante, or any complication, to a mechanical watch, it adds inertia and friction to the system, and thus uses some of the torque of the barrel [42, pp.50]. Figure 6 shows how the torque delivered in a watch declines based on the number of windings of the barrel. It also shows how much torque a simple watch and a watch including a rattrapante needs to keep running. From the figure it is clear that if a rattrapante is added, the total runtime of the watch is reduced.

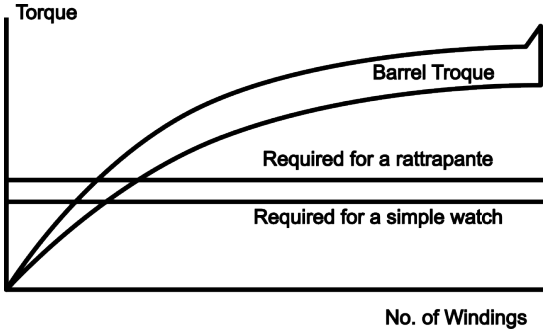

Figure 6: The power output of a mainspring as a function of the number of windings in the barrel, as well as required torque for a running watch and chronograph.

To keep this influence within bounds a criterion has been set: Normally a reference watch runs between 12.0 mNm and 8.00 mNm barrel torque, for this design, the reference watch should still run at 8.25 mNm instead of 8.00 mNm. This thus reduces the runtime, but keeps it within an acceptable range.

This criterion is quantified, however, barrel torque is not a metric that can easily be converted for a concept's feasibility assessment. To get a metric that is easily applied for multiple concepts this torque is converted into rotational inertia. Rotational inertia can directly be applied to anything that runs at the same speed as the rattrapante, and if it has another velocity, it can be converted using the work equation. Using $dW_{max} = \ddot{\theta}\ I_R d\theta$ where $\ddot{\theta}$ is the angular acceleration of the rattrapante.

3.3.2 Base Model

To build a base model of the reference watch, their inertia's, gear ratios and physical connections were put into a Simulink model. The geometry of the geartrain is given in Figure 7, the chronograph and rattrapante are already included to show what the final geometry should look like. Since the test setup where the data was acquired has no hour or minute hand, only the second hand was added in this model.

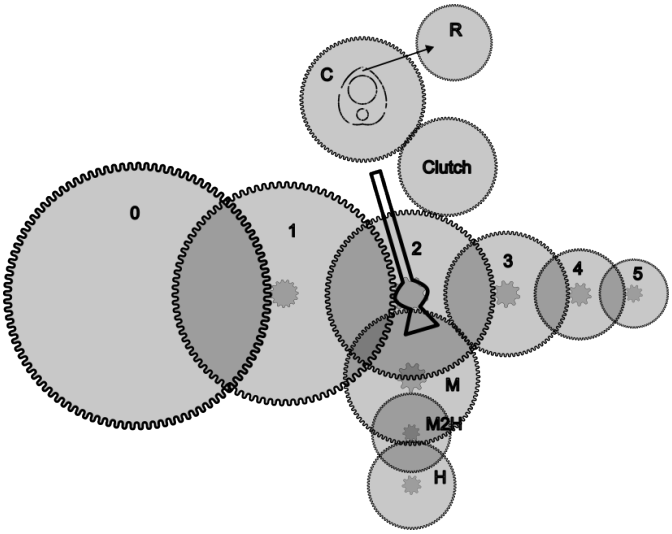

Figure 7: A schematic of the geartrain of the reference watch.

From the reference watch two datapoints are known: they relate the input barrel torque to the acceleration of the escapement wheel. When the barrel torque is 12.0 mNm the acceleration is 40 krad/s^2, and when the barrel torque is 8.00 mNm the acceleration is 20 krad/s^2. Since only two data points are known, the model can only be tuned to two parameters. The main parameters that influence a watch are the friction between the gears and rubies as well as the gear efficiency, η. For this model the friction was simplified to only include the Coulomb friction, $T_{Coulomb}$.

The Matlab® model was build up from simple blocks: the standard Simulink inertia block; a gear ratio block that also takes the gear efficiency into account; a friction block that calculates the dissipated power based on $T_{Coulomb}$ and angular velocity ω; and a rotational power source to simulate the barrel torque input. The output of this model is the angular acceleration of the escapement wheel (Gear 5 in Figure 7).

To check if the computer model is valid the principle of power conversation was applied. For any gear Equation 2 should be satisfied,

$$P_{in} = T_i \omega_i \eta = P_{out} = T_i \omega_i + I_i \omega_i \dot{\omega}_i + \omega_i T_{Coulomb}, \qquad (2)$$

where 'i-1' is a gear in the geartrain and 'i' the following gear, ω the angular velocity and T the torque. Using this equation power conversation was found valid for every gear.

The 2 variables, η and $T_{Coulomb}$, combined with a barrel torque completely define this model. By storing the acceleration of the escapement wheel in a table the two unknown variables were tuned. The values obtained are shown in Table 2.

Table 2: The results of tuning the η and $T_{Coulomb}$ to fit the given datapoints.

Torque (N m)	η (-)	$T_{Coulomb}$ (N m)	Escapement Acc (rad/s^2)
0.008	0.987	4.25e-8	20006.7
0.012	0.987	4.25e-8	39997.3

With these variable tuned, this model runs like the reference watch and the model can now be extended to include a chronograph and a rattrapante.

3.3.3 The Heart

Before adding a vertical clutch chronograph and a rattrapante, a heart cam had to be defined as both the chronograph and rattrapante use a heart cam to be reset to their desired position. The heart was defined in such a way that it resembles the shape shown in patent [70] as the dimensions were provided by an expert as: 2.5 mm center-to-tip, 0.5 mm center-to-bottom and 1.0 mm width of the bottom. A heart shape of these dimensions was defined with the use of the analytical Equation 3,

$$1.5x^2 + y^2 + 0.56|x|y = 1.5^2. \quad (3)$$

The analytical heart is shown in Figure 8 with a hole near the top for inertia reduction as well as a hole for the axis on which is should be placed. In the same figure a red line is shown. This line defines the moment radius if one pushes perpendicular to the heart shape at any point. It is calculated from the normal and the gradient at the force application point. The gradient line is moved to pass through the center of the hole for the axis and the intersection of the normal and the gradient then defines a point on the red line. This moment radius will be needed later for calculations. It also shows why the heart shape is used in mechanical watches. For any point on the right side of the heart, a force applied will generated a moment that will turn the heart counterclockwise, up until the belly of the heart; and for a force on the left side it will turn it clockwise to the belly of the heart.

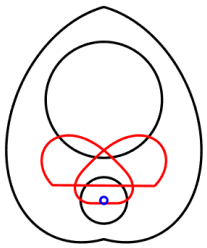

Figure 8: The shape of the heart from the analytical function in Equation 3. The red line indicates the moment radius.

3.3.4 Chronograph and Rattrapante

To add the chronograph and rattrapante accurately, their gears and placement have to be defined. This is done with patent [71] and [72] as inspiration. It is a slight geometric puzzle: the seconds gear has to be moved to a sub-dial away from the center and it is replaced by the main chronograph wheel at the same location which has two hearts attached to its axis. Above it is the rattrapante gear with a spring attached. The spring needs to track one of the hearts (to know where it has to return to once reset) and the gear is needed to be 'grabbed' by the gripper. The resulting geometry is shown in Figure 9, with the chronograph wheel at the bottom and the rattrapante wheel on top.

The image does not show the chronograph clutch wheel. It is a simple gear, designed like patent [73], that is 0.9 times the size of the main chronograph wheel. The data on the inertia's of these extra gears were derived by Solidworks and are shown in Table 3. The inertia of the rattrapante changes based on the position of the heart due to the spring moving in and outward. This was not taken into account and taken as a constant value in the model. At the current position the inertia of the rattrapante wheel is thus an overestimate.

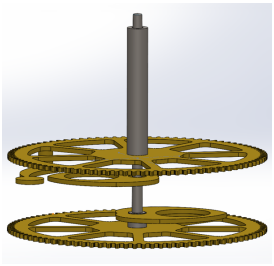

Figure 9: The geometry of the center axis including the rattrapante (top) and chronograph (bottom) gear as well as the hearts and the rattrapante spring.

Table 3: Data on the chronograph and rattrapante gears.

Wheel	Name	Gear # Teeth	Inertia kg m^2
9	Clutch Wheel	90	0.0490e-9
10	Chronograph	90	0.1325e-9
10	Rattrapante	90	0.1389e-9

3.3.5 Criteria check

Using these parts and dimensions a check was performed to see if the 8.25 mNm is a reasonable criterion. To check this, the spring of the rattrapante is tuned to return the rattrapante wheel and a second hand (which would be present in a standard rattrapante) within reasonable time. Since no rattrapante was in my hands, an estimation of the return time of a rattrapante was made based on a video [74]. This video shows a return time of about 0.16 seconds for approximately 175° rotation.

The spring of the rattrapante wheel thus has to be strong enough to return the rattrapante within 0.16 seconds. A simple model that derives the return time was build. It uses the moment radius of the heart and assumes a perpendicular force directed to the axis. A plot of return times for different starting angle is shown in shown in Figure 10. It shows that for a spring stiffness k = 0.05 N/m and a neutral spring length u_0 = 0.2 mm the return time matches the one from the video. Note that in this graph the heart angle is 0° if the tip is pointing upward (as in Figure 8) and that a force is applied from the right. When the angle is 90$degree$ the tip is pointing to the left and the force is acting in the belly of the heart (thus returned).

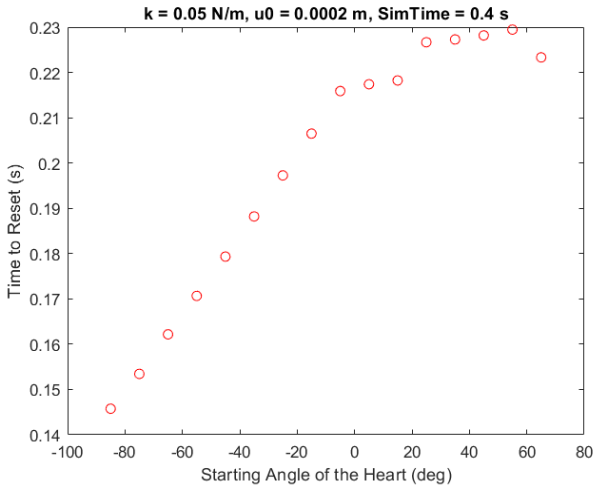

Figure 10: The return time from different starting angles with a spring stiffness of 0.05 N/m

Implementing this spring in the model gives us the acceleration Figure 11. It shows two springs, both with a spring stiffness of 0.05 N/m, one with a neutral length of 0.0 mm and one with a neutral length of 0.2 mm. This is done to indicate the effect of introducing a small neutral length on the acceleration graph. One can see in the figure that the heart shape has a logical influence on the acceleration. One half of the revolution it pushes along, the other half it works against the clock. With a jump seen when it switches direction at the top and the bottom of the heart, and the lowest acceleration occurring when to spring pushes against the top of the heart as the spring has the biggest deformation at that point. Due to the fact that the model can accelerate indefinitely (there is no velocity based friction) this pattern will occur at an ever increasing frequency.

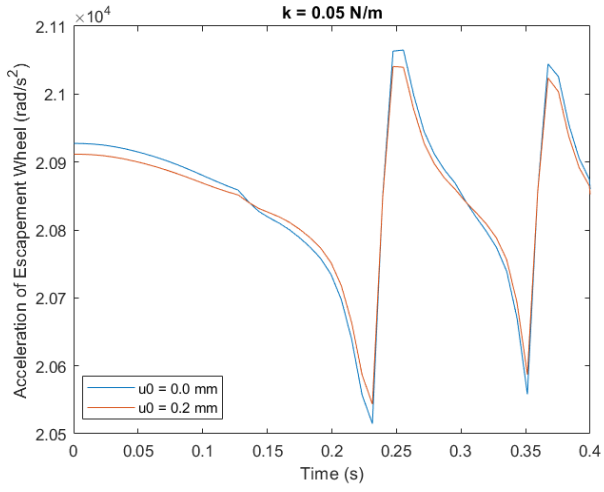

Figure 11: The influence of the heart shape on the acceleration when a spring exerts a force on it during its revolution.

It can be concluded, that a very basic rattrapante can be attached to this clock without dropping the acceleration below 20 krad/s^2. Also, the spring with a neutral length of 0.2 mm was used, since the minimum acceleartion is higher. This would in turn increase the inertia limit.

3.3.6 Limits

The limits of both states, the rattrapante running and the rattrapante stopped, could be found. If the rattrapante is running along it can quite easily be checked how much inertia the rattrapante can exhibit before the acceleration drops below 20 krad/s^2. Figure 12 shows the inertia of the rattrapante and the resulting acceleration. The limit is just slightly higher than 1.4e^{-9} kg m^2.

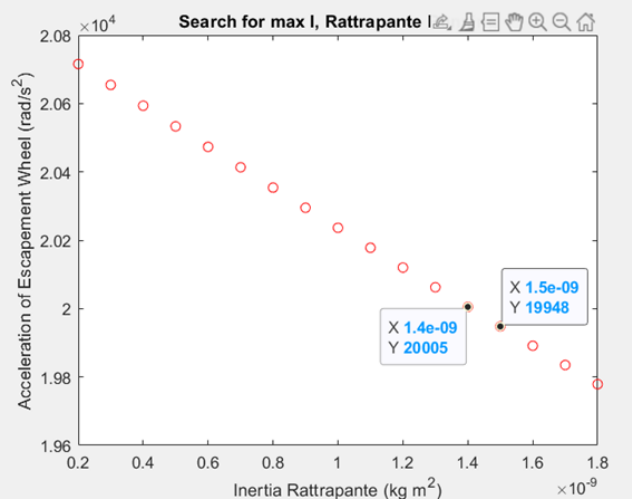

Figure 12: A plot relating the inertia and the acceleration when the rattrapante is running along with the chronograph.

When the rattrapante is stopped it is harder to gain an immediate inertia limit. If the rattrapante is stopped the minimum acceleration is the lowest point in the graph due to the force of the heart, as discussed around Figure 11. The lowest point is extracted and plotted in Figure 13. It shows that 0.145 N/m is the maximum spring stiffness before dropping below 20 krad/s^2. Figure 14 shows the return times for different inertia values returned by a spring of 0.145 N/m. Since the rattrapante still has to be returned within 0.16 seconds, it is concluded that the inertia of the rattrapante should not exceed 0.8e^{-9} kg m^2 when the rattrapante is stopped. One might notice that the accuracy of this plot is not very high. Since the model simply extracted were the angle passes 90° and Simulink uses discrete time steps some data points are extracted when it has already passes for some time.

Since the lower limit has to be taken, this means the maximum inertia of rattrapante can be 0.8e^{-9} kg m^2. However, a small deviation in inertia can be present between running along and being stopped if ever applicable.

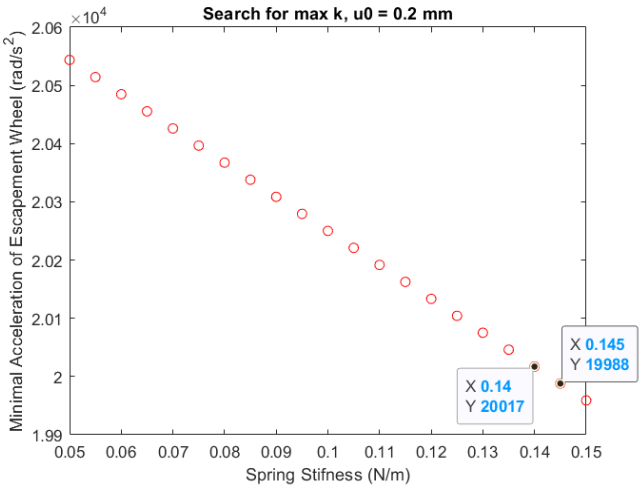

Figure 13: A plot relating the spring stiffness and the lowest acceleration when the rattrapante is stopped.

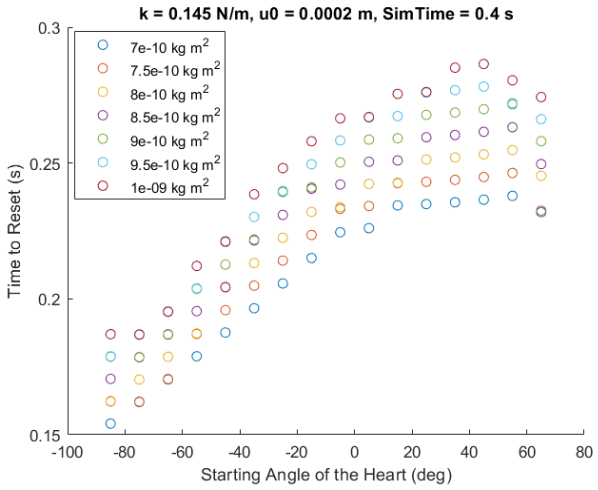

Figure 14: The return times of different inertia's when returned by a spring of 0.145 N/m.

3.4 Other Criteria

Thus far the visibility limit has been defined, the aesthetic value of quite some visual effects has been assessed and the amount of rotational inertia that the design can exhibit is defined. This section will define and quantify the other criteria that need to be satisfied.

Design space The system is allowed to use 1 mm height over the full dial of a 25.6 mm diameter watch. The hour, minute and chronograph hands are located above that cylinder and their axis pass trough its center. Some extra space is available directly underneath. The chronograph module, of 1 mm in height as well, which lies directly underneath, takes up only two-thirds of circle. This space can be used for the rattrapante as well. Figure 15 shows how the design space looks like in a transparent color. As shown, the chronograph space will probably be utilized for the column wheel and gripper. This is a good

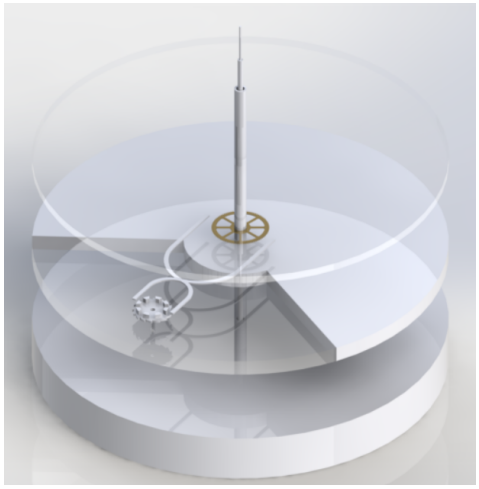

Figure 15: An illustration of the design space (transparent) on top of the watch (opaque).

thing, otherwise the 'actuation' of the visual effect would take up about half of the available height and, due to symmetry, the visual effect would be limited.

The attentive reader might be looking at Figure 9 in 3.3.4 of the friction study and notice that the chronograph wheel is assumed to be on the bottom of the watch there. This is true, and was true at that time. A meeting on the design space after the friction study changed this which made some extra space available. The inertia calculated for the chronograph in the friction study can thus be slightly lower, which would increase the maximum inertia of the system slightly. It was however chosen to omit the work of updating this relatively small change.

Precision Since the design is part of a timing instrument, it should at the least be able to indicate every second.

Assembly The design should be assembleable. Mechanical watches are assembled by human hands. Thus, very fragile parts or parts that would need micrometer alignment need to be omitted, or some way to make assembly possible has to be created.

Patents The watchmaking world is a heavily patented industry. The preceding research concluded that this is should be a feasible project. However, it needs to be checked to guarantee no new patents were published during this thesis as well.

Gravity The visual effect should not be influenced by gravity since watches are worn in all orientations. Thus, if holding the watch in another orientation influences the visual effect or makes the design exceed another criteria (like inertia) the design is not feasible.

3.5 Quantified Criteria List

To summarize, the following criteria list can be compiled. The design should:

- Fit the design space.
- Be aesthetically pleasing.
- Exhibit no more than $0.8e^{-9}$ kgm^2 rotational inertia.

- Only have parts bigger than 90 μm and not 'soak up' contrast.
- Have 1 second indication precision at minimum.
- Be unpatented (and thus be novel).
- Be assembleable by a human hand.
- have little to no influence from gravity.

Furthermore, the following wishes were made. It would be nice if the design:

- Is a compliant mechanism.
- Is produceable from a silicon wafer.
- Improves user experience.
- Decreases production difficulty.

4 Aesthetic Ideas to Concepts

In Section 3.2.3 it was concluded that there were multiple aesthetically pleasing ideas. This section aims to turn these ideas into feasible concepts that fit the criteria. Possible mechanisms were designed and back-of-the-envelope calculations were used to check if they fit the criteria. Based on this analysis, feasible concepts were acquired.

The aesthetically pleasing ideas are discussed in the order of their survey score, starting with the Sine on Circle in Section 4.1, followed by the Ferrofluid Tube in Section 4.2, the Origami Fan in Section 4.3, the Mechanical Mirrors in Section 4.4 and the Loose Ferrofluid in Section 4.5. Section 4.6 and Section 4.7 cover the Magnetic Aiming and Aiming Diamonds ideas respectively, and Section 4.8 gives an overview of the feasible concepts.

Vertical Clutch Some concepts use a vertical clutch to generate extra force. By utilizing the power from a the button push, a gear is pushed upward (or downward). By using this on the rattrapante gear, some extra force can be generated that is not supplied by the barrel and thus allows some concepts to circumvent the inertia limit.

A vertical clutch is shown in Figure 16. In Figure 16a and 16b it is shown in disconnected position and in Figure 16c and 16d in connected position. When the clamps (21) and (22) move together, they push a gear (9) up. The upward movement can be used an actuating force.

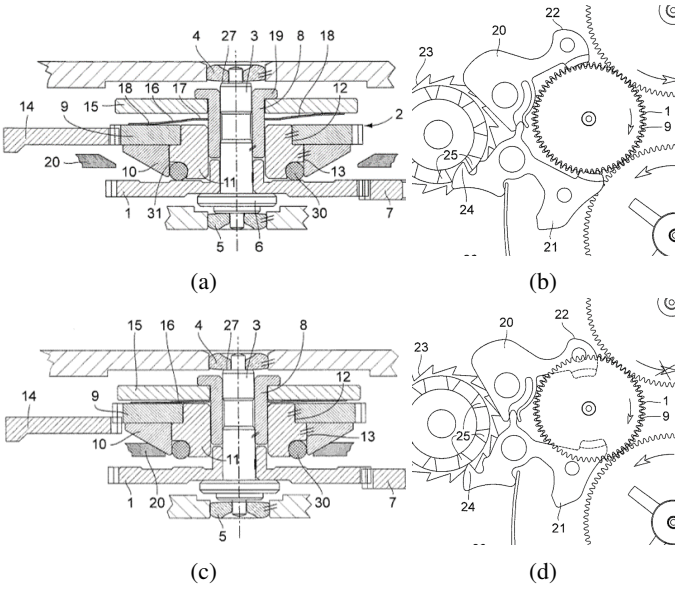

Figure 16: An unengaged a) side and b) top view and an engaged c) side and d) top view of a vertical clutch [44]

4.1 Sine on Circle

This section will explore various ways to achieve the sine on circle effect shown in Figure 17

Initially, there seem to be a couple of possible ways to achieve this effect and they will be explored in this order:

- By utilising a Moire effect
- By buckling parts of a circle
- By rotating the entire effect with the system
- By flipping the sines in and out of plane

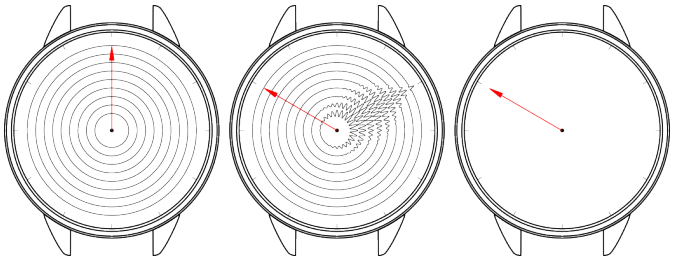

Figure 17: The original Sine on Circle idea

Moire Effect Moire effects are visual effects that overlay two 'planes' of lines over another to create shapes or patterns. Dr. Oster wrote a book about their physics, one can use the effect he describes to generate the effect shown in Figure 18 [75, p.29] . It can be tuned into a polar effect with the desired dimensions to indicate the seconds.

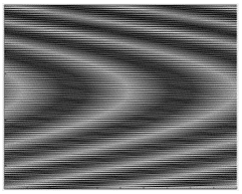

Figure 18: A Moire effect that generates a sinusoidal pattern.

This effect requires a layer of straight lines and one off slightly angled lines. Both on a transparent disc. One of them would be required to rotate along with the rattrapante while the other is stationary. For this back-of-the-envelope calculation it is assumed it needs a 1 to 1 speed to indicate every second. A solid plastic disc (ρ=1000 kg/m$\hat{3}$) disc with a diameter of 25 mm (slightly smaller than the watch face) that has a maximum inertia of 0.8e-9 kg m$\hat{2}$ could have a maximum thickness of 50 μm. Which seems thick enough to achieve the desired result and be statically stable. So, using a Moire effect could be a feasible concept.

Rotating Rings One might also be able to create the rings with the sines already on them. The wont disappear if the mechanism is inactive, but it does generate the sines. These rings would be connected to each other with a thin structure and simply rotate along. It can almost exactly recreate the original effect. Neglecting the inertia a sine would add the the circle, a ring's inertia can be calculated from $I_{ring} = 0.5\pi\rho t \cdot (r_{out}^4 - r_{in}^4$. The inertia of 10 rings equally spaced between 4 and 12 mm radius with a thickness of 30 μm, a width of 200 μm (for visibility) and a density of silicon (ρ= 2330 kg/m$\hat{3}$) becomes 0.59e^{-9} kg m^2. This fits the inertia criterion and leaves room for rigid connections between the circles. So, using a rotating rings could be a feasible concept.

Buckling One could also try to buckle parts of a stationary ring to generate this effect. The buckling force would need to be applied from the center. Creating a pre-buckled system could also a possibility. Some sort of bi-stable mechanism would have to be created, where an 'invisible' pre-buckled sine unbuckles to buckle a visible piece. However, these ideas simply sound like they will give a lot of problems, space-wise and force-wise. These ideas are thus marked as not feasible.

Flipping out of plane Another idea would be to create sines that are standing 'up', perpendicular to the dial plane, and flip them to be in that plane. 60 sectors of these sines would need to be created, so each second is inidcatable. Figure 19 shows how this would look like from the top.

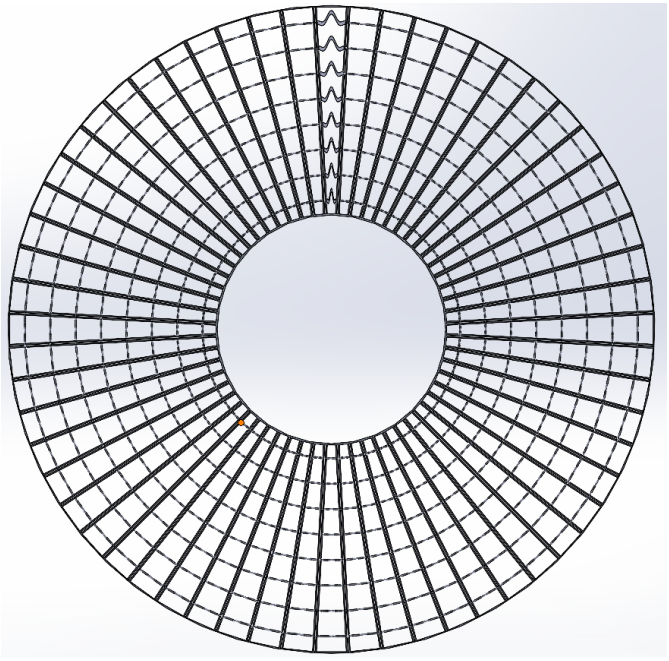

Figure 19: A top view of how the flipping sines would look like.

To achieve this the vertical clutch could be used to push a bar upward which in turn would flip the mirrors. Figure 20 shows a mechanism that could achieve this. This also means the power to flip the sines would be provided by the button push and not by the mainspring.

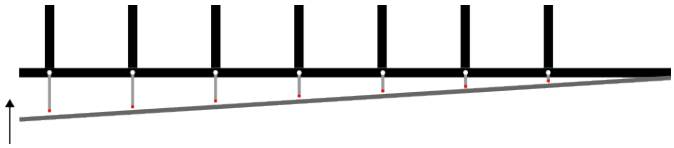

Figure 20: A schematic of the actuation by a vertical clutch of the flipping sines.

To make sure this is assemblable, without the need to place every sine (about 600) of micrometer size trough a hole or something in that precise manner a construction method has been though of in advance: Two frames of minimal thickness are created with slight half-circular indents in the top or bottom. A grid with all the sines can be produced with very thin connections between them. Connections of such a small size that they can only barely hold the structure together when lifted. That structure can be placed in between the 2 frames in the indents. In which is should fit almost exactly. Once the two frames are 'glued' together, a force can be applied on the sines to break the thin connections. After which the sines are free to make their desired movement.

This idea is quite difficult, but can achieved, and is thus marked as a feasible concept.

4.2 Ferrofluid Tube

This concept is based on a ferrofluid in a tube that is driven by a permanent magnet. It is shown in Figure 21.

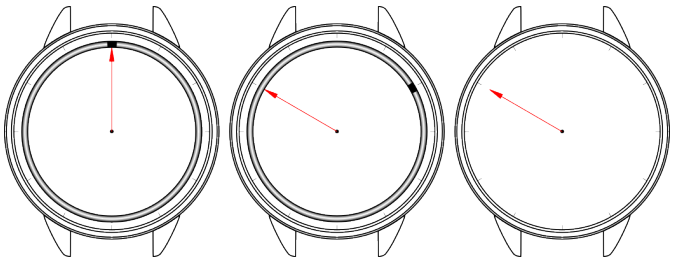

Figure 21: The original Ferrofluid Tube idea.

For calculations, it is assumed that the tube is 12 mm in radius. It contains a cylinder of fluid with 0.3 mm diameter and 0.3 mm length (to satisfy visibility requirements) and it is assumed to have the density of water (even though the magnetic particles will make in denser). Neglecting fluid friction with the wall, this mass would need 6.2e^{-9} N of force to move it 6 degrees in 1 second.

The magnet could be a NeFeB magnet (the strongest commercially available) that would need to be placed on a needle to be as close to the fluid as possible (magnetic fields decrease with r^{-4} and inertia is added with r^2). Assuming a 1x1x1 mm magnet [76], subtracting the moment (force needed times radius) needed for the fluid and subtracting the inertia of the rattrapante

gear (0.139e-9). The magnet can at maximum be placed 8.5 mm from the center.

Comsol is used to evaluate the magnetic force on the fluid. The fluid is assumed to be magnetized according to the formula $M_{ferrofluid} = 17200 \tan^{-1}(0.000016\,H)$ [77]. The magnet has a residual flux density $B_r \approx 1.21T$ [76]. Using the parametric sweep function of Comsol, the data shown in Figure 22 is returned for a sweep over theta for 0 to 2pi/60. The force, of about $2e^{-6}$ N, is big enough to push the fluid.

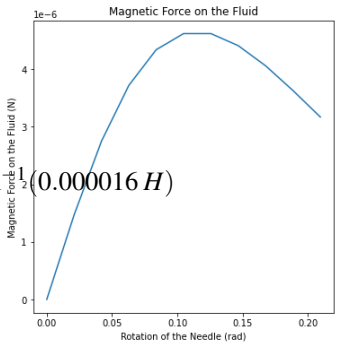

Figure 22: The magnetic force on the fluid based on the angle between the needle and fluid.

This concept is thus feasible. However, if the rattrapante is reset, it will have to be reset slowly. The fluid is much 'slower' than the needle, and if the needle is to far away the fluid will stay stationary and wait until the magnet return to the position where it currently is. This is a negative aspect which will later be taken into account in Section 5.

4.3 Origami Fan

This concept is based on the origami herringbone tessellation [78]. The idea is shown in Figure 23. Origami seems like the most feasible way to achieve this, either in one piece or multiple pieces.

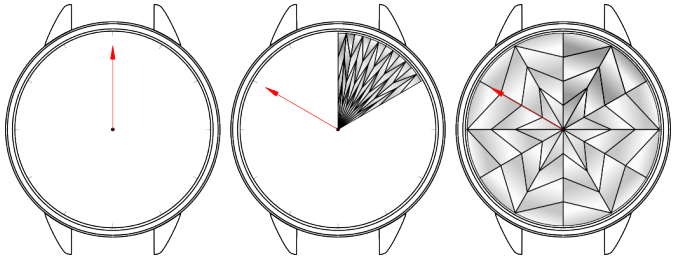

Figure 23: The original Origami Fan idea.

One piece The idea takes on herringbone tessellation and folds it all the way around with a total of 60 sectors. On the outside, $1/60^{th}$ of the radius is 1.34 mm. Due to the height limits, this could not be folded all the way back (each fold will become vertical), thus this idea would need 120 folds.

If all 120 folds are folded back together, and assuming a thickness of origami paper of 50 μm [79]. The thickness of a folded stack is 6 mm. This means that at the outer edge more than 4 seconds can not be indicated. At the inner edge the 6 mm thickness generated will make this idea look bad aesthetically. Thus using a single herringbone tessellation over the entire dial is not feasible.

Multiple pieces One could split the tessellation into 60 pieces to indicate each second with a segment. Assuming each segment is pushed at its center of mass at 8 mm distance from the center, using a grammage of 45 g/m^2 [79] and assuming half of the acceleration of the rattrapante: a segment would need $27e^{-6}$ Nm torque. The torque delivered to the rattrapante is only $11e^{-6}$ Nm. Making this concept not possible.

4.4 Mechanical Mirrors

The mechanical mirrors concept is shown in Figure 24. It is based on tilting mirrors to achive reflection and a height difference at the same time.

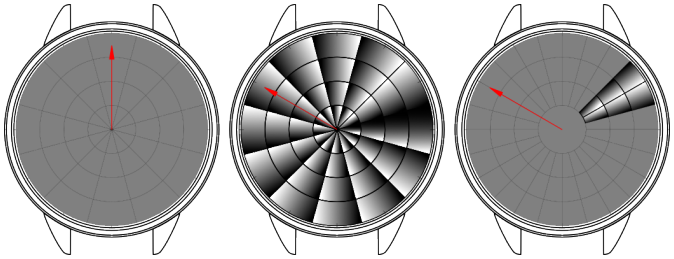

Figure 24: The original Mechanical Mirrors idea.

From the survey it is clear that the third image is the more clear and the most aesthetically pleasing. So, this concept should fold 2 planes outward. The simplest way to achieve this shown in Figure 25. Figure 25a shows the mirrors an in unexcited state. By pushing against the compliant hinge, the mirrors can be actuated to an angle as shown in Figure 25b. By using a vertical clutch one could push a bar against the hinge, the power to flip the mirrors will then be delivered by the button push and not the barrel. This concept is quite simple, but most definitely feasible.

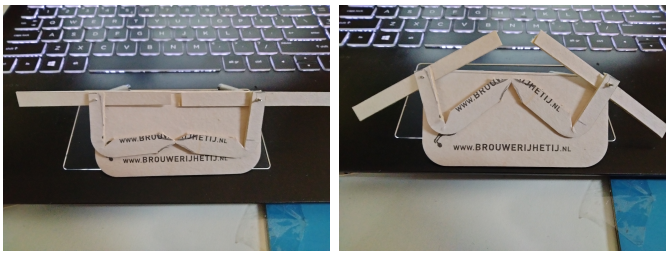

(a) (b)

Figure 25: A cardboard model of how actuation of the Mechanical Mirrors can be realized.

4.5 Ferrofluid

The idea is shown in Figure 26. It was thought of with a free flowing ferrofluid in mind.

It is however not a feasible concept. Apart from the struggle that loose fluids in watches create. This idea needs an electromagnet. If two permanent magnets are used. The fluid will find a stable equilibrium of 2 'blubs' around their poles. What the

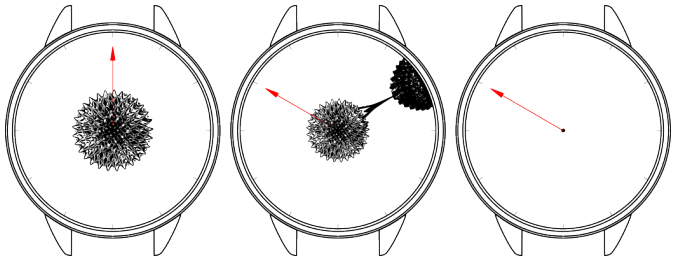

Figure 26: The original Ferrofluid idea.

strength of this idea is, is that the flowing fluid from the center to the edge indicates the time. Also, a loose 'blub' of fluid is not precise enough to indicate a second precision. It is thus discarded.

4.6 Magnetic aiming

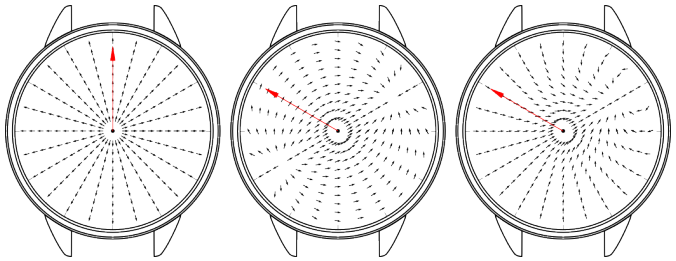

Figure 27: The original Magnetic Aiming idea.

The Magnetic Aiming idea is shown in Figure 27. It aims needles based on magnetic field lines.

Before calculations on this design are made two things are changed: the needle size and the magnet location. From the aesthetic survey it became clear that the small needles are quite hard to see. So, just like the Aiming Diamonds, the needle size is varied based on the radius. The magnet location is moved closer to the center. This was done for both inertia as well as magnetic field reasons. If the magnet is closer to the center it takes less power to move and the distance to the other side of the watch becomes smaller, thus it needs a smaller magnetic field. The effect after these two changes is shown in Figure 28, it aims at 45 seconds and has the magnet poles located at 1 and 3 mm radius.

All these needles need to be able to rotate separately. Normal compass needles sit on a pivot that generate almost no friction. However, these pivots do not work if a compass is tilted, and are thus not fit for a watch. For the purpose of this concept, a bearing idea is designed that should have very little influence of gravity, it is shown in Figure 29. This ruby bearing will have quite some friction which has be taken

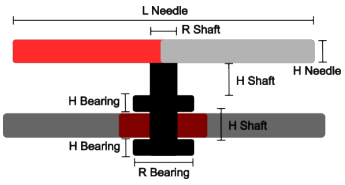

Figure 29: A schematic of the bearing for the needles.

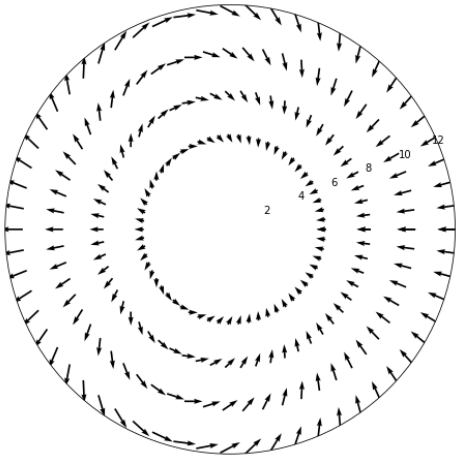

Figure 28: The revised Magnetic Aiming idea.

into account. The dimensions of the bearing are set at: R_{shaft} = 0.20 mm, $R_{bearing}$ = 0.25 mm, H_{shaft}= 0.2 mm and H_{needle} = 0.1 mm.

For the calculations the following assumptions were made:

- The magnet is a dipole. This is not entirely valid for some of the closest needles, but these are also the needle with the biggest magnetic force / force needed ratio.
- The direction of a needle is given by the direction of the magnetic field B. The magnetic field B is given by Equation 4 [80, p.149],

$$\mathbf{B}(\mathbf{r}) = \frac{\mu_0}{4\pi}\left[\frac{3\mathbf{r}(\mathbf{m}\cdot\mathbf{r})}{r^5} - \frac{\mathbf{m}}{r^3}\right], \tag{4}$$

  where μ_0 is the vacuum permeability, $\mathbf{r}$ is the vector from the center of the magnet to the point where $\mathbf{B}$ is measured and $\mathbf{m}$ is the magnetic moment of the magnet.
- Magnetic torque τ on the needle as a result of the magnetic field of the magnet $\mathbf{B}_1$ is calculated using Equation 5 [81, p.276],

$$\tau = \mathbf{m}_2 \times \mathbf{B}_1, \tag{5}$$

  where $\mathbf{m}_2$ is the magnetic moment of the needle.
- A needle moves from stationary position at angle θ_1 to stationary position at θ_2 in 1/80 seconds (frequency of the watch). This removes the need for kinetic energy in the work equation. For each of the 4800 steps dθ is shown in Figure 30.
- Friction with the ruby, μ = 0.15 [82], is based on two things: rotational friction between the ruby and shaft, and Coulomb friction with the bearing and shaft due to gravity. Rotational friction is added as an extra opposing force to the torque needed as $1 \cdot (I\alpha) + 0.15 \cdot (I\alpha)$. Coulomb friction is calculated using $m_{needle}\ \mu\ g\ r_{shaft}$. Bringing the total torque required to $T_{needed} = 1.15 \cdot (I\alpha) + T_{Coulomb}$
- The magnet is a NeFeB magnet of size 1x1x2 mm.

Per step 60 needles have a $d\theta$, their summed work should not be more than the maximum work delivered, which is 1.75e-10 J. Summing the work of the needles shows that they use 1.31e-10

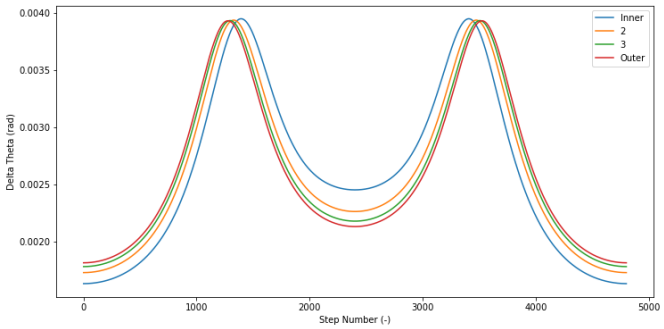

Figure 30: A plot of dθ for every step in a full minute rotation of the different needle bands.

J. Which translates to 1.98e-10 kg m^2 rotational inertia left for the magnet and gear. At the prescribed position, the magnet and gear have a rotational inertia of 1.90e-10kg m^2. So, this should just fit the inertia criterion.

The question remains, is the magnetic force big enough to actuate the needles. Figure 31 shows the torque required and the torque delivered by the magnet. The magnetic moment of the needles are 2e-7, 1.5e-6, 9e-6 and 3e-5 A m^2, from the inner to the outer ring respectively. These were mainly chosen to fit the graph nicely. Also, 3e-5 A/m should easily be reachable as compass needles can have 60 A m^2 magnetic moment [83].

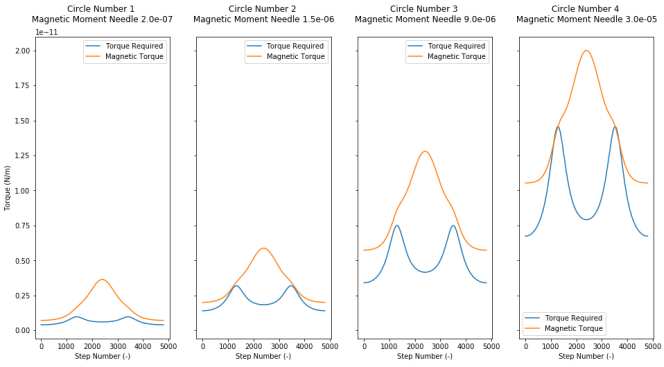

Figure 31: The torque required vs the torque delivered by the magnet for each of the needle bands.

Even though questions should be raised about the assembly of 240 needles in a dial, this concept is feasible.

4.7 Aiming Diamonds

The Aiming Diamonds idea, shown in Figure 32, aims diamond shapes basedd on the gradient to the incication point.

The main commentary form the aesthetic survey is that the diamonds shape is not pretty, but that the aiming itself is nice. The diamonds are thus replaced with needles whose sizes vary with the radius. There are three main possibilities to achieve this effect, which will be discussed in the following order:

- Non-circular gears
- Grooved rotating disc
- Spring based actuation

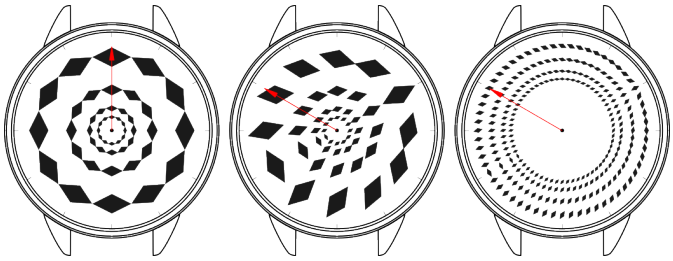

Figure 32: The original Aiming Diamonds idea.

Non-circular Gears To achieve this effect mechanically every diamond would have to be on its own, non-circular, gear and would also require an intermediary gear to get clockwise rotation for all of the diamonds. Each gear has its own efficiency and inertia, and knowing there is only 12 (including the rattrapante) gears in this watch, adding multiples of 120 does not seem feasible.

Grooved Disc An option could be to use a grooved disc in which the diamonds are guided. Using almost the same bearing, only adding a little knob to fit in the groove, as in Figure 29, and using the same work and friction calculations as used in Section 4.6 for the magnetic needles, the inertia left for the grooved disc can be calculated. The work needed is evaluated at 8.69e^{-11} J, with 1.75e^{-10} J supplied to the rattrapante, the work left can be converted to 4.02e^{-10} kg m^2 inertia for the grooved disc. Using the inertia of a disc results in a thickness of 19 μm of this grooved disc (assuming ρ=1000kg m^3). This is to thin for a force bearing disc that is only supported at its center. Thus, using a grooved disc is also not a feasible concept.

Spring Based One could also try to move a hand below the surface to which all the diamonds are connected to by very light springs. These springs would need a very low spring stiffness, as well as a very long maximum elongation. Another problem that arises is the geometric fit: all these springs would need to be at different heights to ensure that they are not intertwining. This intertwining should also be prevented at the tip of the needle where these springs all connect to the same point. All three problems, at this scale, add up to an unfeasible concept.

The Aiming Diamonds does not generate a feasible concept, and will thus be discarded.

4.8 Feasible Concepts

By researching possible mechanisms to achieve all the aesthetically pleasing ideas generated and surveyed in Section 3.2 six feasible concepts were created that should fit the criteria:

- Sine on circle
  - Moire Sines
  - Rotating Sines

  - Flipping Sines
- Ferrofluid Tube
- Mechanical Mirrors
- Magnetic field

These concepts will be weighted and compared to make a substantiated choice in Section 5.

5 Concept Choice

The 6 feasible concepts created in Section 4 are compared by using a weighted criteria table. The criteria weighted are:

- Friction (4): If the concept has less friction/inertia/work needed the watch runs longer. Also, if less friction is present in the concept, there is more room for deviation in the final design.
- Accuracy (3): All concepts have at least the minimum 1 second precision. However, some concepts might have a worse readout accuracy or a slower readout. This is undesirable.
- Novelty (3): Some effects are less novel in the watch-making world, that novelty in such a niche industry is important. The novelty also takes a bit of 'wow-factor' into account.
- Visibility (2): Based on the size of parts the concept might be better visible from different angles or from further away. Both of these are positive for a watch.
- Gravity (2): The concept should not be influenced by gravity in a way that either friction or underconstrained parts might break the concept.
- Assembly (2): If the watch has a lot of parts, very small parts or very fragile parts, assembly will take more time and will thus be more expensive.
- Minus (1): For the return time of the Ferrofluid Tube points are subtracted.
- Aesthetics (1): The aesthetic score is determined by the survey in Section 3.2. Since these scores are between 10 and 16 a weight of 1 was given to not skew the weighting table.

All concepts get a score between 1 and 5 based on all of these criteria (except aesthetics as explained). The scores are shown in Table 4. An elaborate explanation of why these scores were assigned can be found in Appendix C.

Final Choice From the table it is clear that either 3 of the following concepts should be chosen:

- Separate Sines
- Flipping Sines
- Mechanical Mirrors

Corresponding with thesis deadlines, a presentation was given for the supervisors of this project. At the end of this meeting a debate took place about these three concepts. During this debate it became clear that the Separate Sines might not be the best concept because it is not dynamic. The sines do not move as was in the original idea. This makes it less aesthetically pleasing. It also became clear for the Flipping Sines people saw risks ahead. Even though an assembly method was devised in Section 4.1, these parts might beto fragile for assembly as well as a chance of failure during transport or possible shocks while worn. These risks combined made us doubtful of the concept.

However, for the Mechanical Mirrors all of us saw potential. Due to the simplicity of the current concept with a single compliant hinge and the assembly which would not consist of too many and not too fragile parts. We also saw potential in possibilities for changing mirror orientations and the number of mirrors.

Table 4: The feasible concepts are compared against each other based on different weighted criteria. By giving a value between 1 and 5 multiplied by the weight of the criterion and adding the weighted scores gives a total score for comparison.

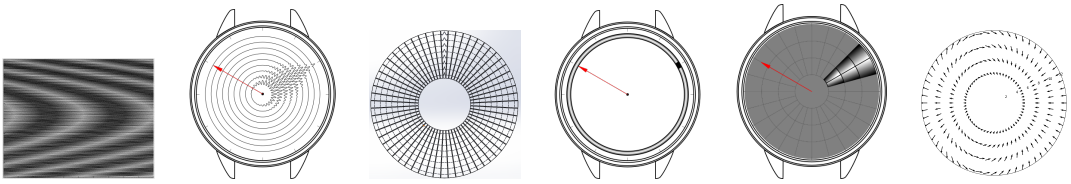

Criterium	Weight	Moire Sines		Separate Sines		Flipping Sines		Ferrofluid In Tube		Mechanical Mirrors		Magnetic Field	
Friction	4	3	12	4	16	5	20	4	16	5	20	2	8
Accuracy	3	3	9	5	15	4	12	2	6	4	12	1	3
Novelty	3	1	3	3	9	5	15	4	12	5	15	5	15
Visibility	2	3	6	5	10	4	8	5	10	5	10	4	8
Gravity	2	5	10	5	10	4	8	4	8	5	10	3	6
Assembly	2	5	10	4	8	2	4	2	4	3	6	1	2
Minus	1		0		0		0	-3	-3		0		0
Aesthetics	1	16	16	16	16	16	16	15	15	11	11	10	10
Total			66		84		83		68		84		52

So, we decided that the Mechanical Mirror concept would become the final design. The one main takeaway from the discussion is that before turning it into a final design, different mirror orientations should be explored. This will be done in Section 6.1

6 Design

With the Mechanical Mirrors concept as the final choice it has to be turned into a working design in this section. From the feedback it is clear that flipping mirrors can be done in multiple orientations and should be researched before continuing with the current concept.

First, the possible mirror orientations will be explored and an initial design will be created in Section 6.1. After that, in Section 6.2, a production method will be established, this production method along with the criteria will be used to define the main dimensions of this design in Section 6.3. Section 6.4 will be dedicated to the stress in the flexures followed by Section 6.5 where a hinge used in Section 6.1.3 is redesigned. Section 6.6 designs an actuation mechanism and Section 6.7 fits the entire mechanism into the design space.

6.1 Final Visual Effect

To explore possible mirror orientations multiple prototypes were 3D printed to analyse their behaviour and their generated effect. Simply put there are two main directions in which the mirrors can be rotated, taking the 60 second mirror as reference (the one facing 12 o'clock), mirrors can be rotated around the x or the y axis to generate movement out of plane.

6.1.1 Possible Mirror Orientations

The original concept was created with rotation around the y axis and was named the 'In-Out' effect. A prototype is shown in Figure 33a and the rotation is achieved by rotating the mirrors over the full length of the dial around a compliant torsional hinge.

Rotation around the y-axis is less straightforward. If a single mirror is used, the maximum angle is very small before the height limit is reached. Also, for an odd number of mirrors the force can not be purely axial. The mirror is thus split up in even number of pieces, alternating between positive and negative rotation. This effect was named 'Up-Down', and is shown in Figure 33b with four mirrors. A second possibility with rotation around the y-axis is creating an 'Arc' that is shown in Figure 33c. The arc takes up more height than 'Up-Down', it is however a more stable excited state.

A choice has to be made between these possible rotations. The In-Out movement is the simplest variation. It can be actuated by the vertical clutch as described in Section 4 directly and a hinge to achieve this has already been thought of in Section 4.4. The Arc and Up-Down variations are more difficult to actuate, the vertical force of the clutch has to be converted into a horizontal force. However, that should however be achievable by a simple conversion mechanism.

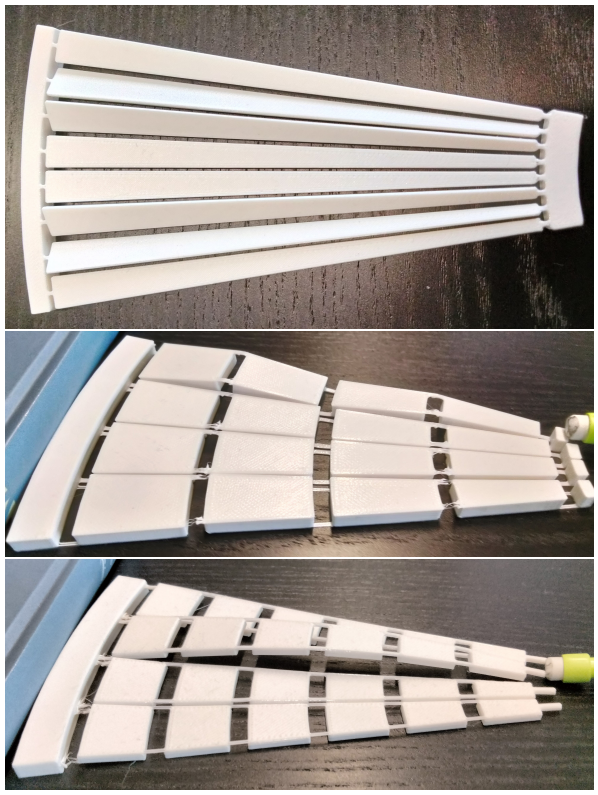

Figure 33: Possible orientations: a) In-Out, b) Up-Down and c) Arc.

Another difference between the In-Out, and the Up-Down and Arc orientations. Since the In-Out has mirrors over the full length of the dial, they can not be split in over the length. The Up-Down and Arc on the other hand have quite some variations possible. For both of them the amount of mirrors can easily be varied. The Arc can also change the length of the different segments to change the shape of the arc itself. The Up-Down can change the length of mirror pairs to create different sized hills or the length within a mirror pair can be varied. If the length of a pair is varied by using a long and short mirror the short mirror might achieve a vertical position or even overshoot it's own bottom.

Even though none of these differences are a criterion, the choice was made on personal preference. The fact that the amount of mirrors and their lengths can be varied for the Up-Down without gaining a lot of height (which is the case for the Arc inherently) makes this orientation more fun (Also, the challenge the Up-Down gives makes it more fit for a MSc Thesis).

6.1.2 Constraints

The Up-Down effect has one big problem at this moment: it is underconstrained by multiple Degrees of Freedom (DoF). Currently, the high and low flexures between the mirrors generate a moment and should ensure a correct rotation direction. However, due to the fact that the mirrors are underconstrained, two

undesired things happen. Figure 34a shows a situation where the mass of the mirrors is not big enough to keep the flexures from pushing it upwards. This generates a 'bad' type of arc shape. Figure 34b shows another situation where the only one of the mirrors pairs is actuated. Since the moment on the flexures becomes bigger if their angle is bigger, the other pair will never leave the surface.

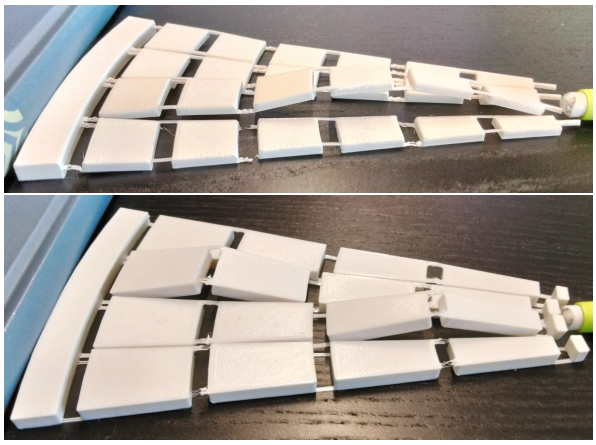

Figure 34: The effect of an underconstrained mechanism: a) undesired Arc shape, b) only one mirror pair actuated.

A constant and repeatable actuation of the system is needed, so only one DoF should be present. Assuming the mirrors are on a flat surface, one could try to generate a force against this surface. This will make sure the mirrors always actuate in the right direction, removing the problem of Figure 34a. It will however not constrain the problem shown in Figure 34b. Another possibility would be to create a 1 DoF sliders on the lower hinges, one could once again remove the problem in Figure 34a. To remove the problem in Figure 34b, these sliders would need a limit on their movement. These sliders however would need to be very small and fragile, which is not desired for something that would need to also bear force.

6.1.3 Scissors

The most straightforward solution is to create a scissor mechanism. By creating more rows of mirrors per indicated second, one can connect the mirrors on their rotation point by a torsional member. This constrains the system to exactly 1 DoF (assuming the force applied is strictly horizontal). Another positive of these hinges is that the mirrors do not need any contact surface except the outer edge. They can thus be floating above the mainplate.

Figure 35a shows the top view of 2 mirror segments at rest. In the Figure it can be seen that the outer flexures are only half of the mirror width to ensure symmetry in flexure forces. One can also see that the edge flexures are longer than the flexure between the mirrors. This is for the simple reason that the outer edges need to buckle, which creates more stress than simple bending. Section 6.4.2 and 6.4.3 dive deeper into stress in these flexures. Figure 35b shows a side view of a working prototype of these scissored mirrors in actuated state. It can also be seen that the mirrors still alternate between the top and bottom of the mirror.

This top view is also in the standard orientation. With the outer edge on top and the inner, actuated, edge on the bottom. The hinges are counted from the inner edge to the top.

Figure 35: The a) top view and b) actuated side view of the scissor mirror.

6.1.4 Mirror Density

The scissor design allows for an odd number of mirrors. As shown, this prototype contains three. The amount of mirrors has influence on three things: the 'mirror density', the angle of rotation achievable and the actuation displacement needed. The mirror density is defined as the amount of space occupied by mirrors versus the amount of space occupied by flexures. If the mirror density is higher, less gaps are present in the top view. These gaps are not inherently bad, but personally, limiting them to the minimum seems more aesthetically pleasing. The angle of rotation is mainly related to the amount of mirrors. The more mirrors are present, the bigger the maximum rotation becomes. The bigger the maximum rotation, the bigger the angle of the flexures and thus more stress if the flexure has to same length. Thus, more mirrors means longer flexures and thus a lower density. However, a smaller rotation of the mirrors makes the effect less visible based on reflection. The angle of rotation also in-

fluences the actuation displacement required. The vertical displacement of the vertical clutch will be limited, thus a very big displacement is undesired.

That is why this design currently takes three mirrors. With an approximate angle of 15deg, it needs about 0.24 mm displacement to reach the height limit. Combined with the mirror density of 3 mirrors this seemed optimal.

6.2 Production

The initial design of the Scissor Mirror mechanism is complete. However, it also needs to be produced. This mechanism nearly impossible to produce using conventional production methods due to its size and shape. A wish was made in Section 3.5 to create a design that was produceable from a silicon wafer. This section will thus explore how the production of this mechanism can be achieved. Section 6.2.1 will cover the etching of silicon wafers. Section 6.2.2 will introduce BOX layers and the mechanical properties of silicon wafers are explored in Section 6.2.3. Section 6.2.4 will conclude the production section with the reflective properties as well as the colors achievable when using silicon wafers.

6.2.1 Silicon Wafer Etching

SOI wafers can be dry or wet etched. Dry etching is done perpendicular to the top plane, it is used to remove material and leaves cavities with near vertical walls [84, p.208]. The depth of such an etch is hard to accurately control, thus it is normally used to cut through the entire wafer. Wet etching is also done perpendicular to the plane, but instead of vertical walls, it generates walls under an angle [85]. The dry etching technique is more fit for this design due to the vertical walls and will thus be used. It gives two problems however: the first is the fact that the depth needs to be controlled; the second that it needs to be etched from both sides (since one can not etch through a flexure)

The second is not really a problem, an dry ethcing machine can turn the wafers itself, and has a misalignment of about 70 nm [86]. It limits the minimum size, but on 10 μm structures it is not significant.

6.2.2 BOX layers

The depth control of dry etching is a problem. The flexures need a very specific thickness that is equal over all the flexures to ensure smooth stress distributions. A solution for creating cavities of a certain depth are Buried Oxide (BOX) layers. They are oxide layers that act as a chemical stop for the etching process [84, p.208]. After the BOX layer is reached, the layer itself can be removed by another process that does not influence the silicon wafer. These steps are shown schematically in Figure 36 by red and green arrows respectively.

The flexure thickness is defined by the film thickness, the layer on top of the BOX layer. [84, p.208] reports the most common range of the film thickness to be between 5 and 20 μm. They also report that the BOX layers range between The BOX layer thickness is reported between 0.5and 2 μm.

However, this design would need a wafer with 2 BOX layers, since the flexures are both at the top and at the bottom of the wafer. Double BOX layer wafers are not as easy to buy commercially as wafers with none or one BOX layer. However, people have created them for their own experiments [87]. Also, companies like Okmetic produce wafer with 2 BOX layers stacked on top of each other with cavities between them [88].

So, a double BOX layer wafer exist and should be availible. The production, using dry etching, BOX layer stripping and a wafer rotation would schematically look like the one shown in Figure 6.2. It does include multiple some steps, but it should be possible to achieve.

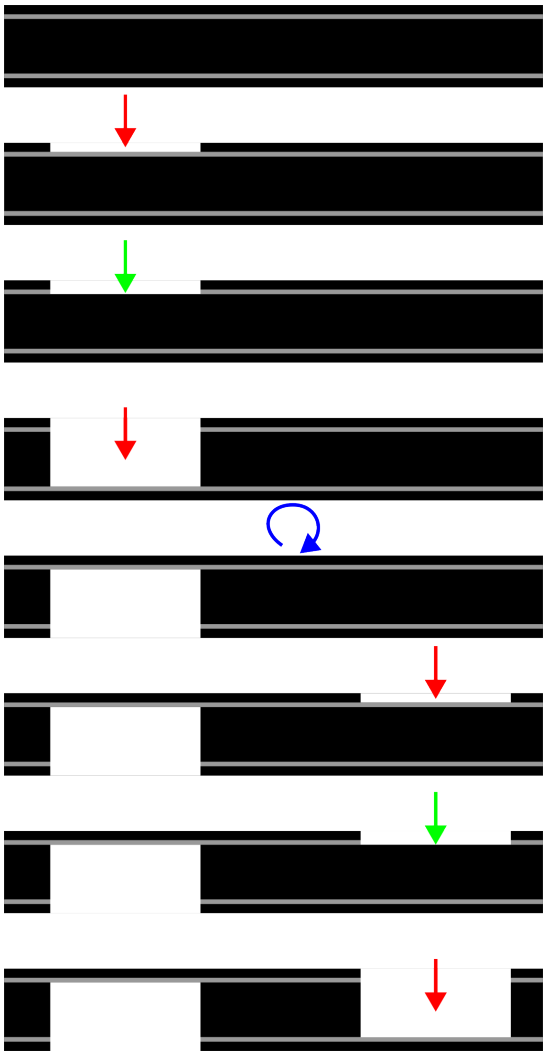

Figure 36: An illustration of the approximate production steps. With the red arrows indicating a dry etch, the green arrows indicating an oxide etch and a wafer flip in blue.

It does raise one other problem though. The current hinge that constrains the system is in the middle of the mirrors. Using extra BOX layers would bring the total up to four layers. Since

double BOX layers are already not really common, it should not be stretched. Also, it would more than double the amount production steps. This torsion hinge will thus be redesigned in Section 6.5.

6.2.3 Mechanical Properties

For stress calculations the following properties are needed: the Young's modulus, Poisson ratio and yield strength. Silicon wafer properties are not straightforward. They vary greatly for different wafers based on crystal orientation and surface finish. "Mechanical strength of Si wafers depends more on the surface condition or the length and number of micro cracks than on the surface orientation." [89]

A choice was made for the CO14018 wafer from 'Siegert Wafer' [90]. Those wafers have a 300 μm thickness, are finished with a double sided polish and have a <100> crystal structure. Some sources were collected to find representative values for the mechanical properties of these wafers.

Hopcraft states that "the possible values for Young's modulus range from 130 to 188 GPa, and those for Poisson's ratio range from 0.048 to 0.40." [91]. Figures in the paper show that for <100> wafers the Young's modulus is 130 GPa and the Poisson ratio is 0.28.

Silicon is a brittle material, thus the fracture strength and Yield strength are very close. The reported values vary greatly: between 960 MPa [92] up to 7.2 GPa [93]. However, as stated above, the surface cracks and surface condition influence the strength. For safety a limit of 800 MPa as a yield strength was set. Since silicon is a very brittle material, which will fail in tension rather than compression, compressive stress can overshoot this limit slightly.

6.2.4 Color and Reflection

Another positive of using silicon wafers a a production material are the color possibilities and reflective properties. One can change the color of a silicon wafer by adding a silicon or nitride film of a specific thickness on top of it [94]. Almost the entire color spectrum is possible, allowing for a highly customizable visual effect for different customers [95]. Also, silicon wafers are vey reflective, they are even used in reflection and detection measurements [96]. This will improve the contrast and visibility of this design.

6.3 Dimensions

This section will use the production method and some criteria to define dimensions of the design.

Outer Edge To fit the design space, the outer measurement can be 12.8 mm in radius. Taking this as a dimension makes sure that the entire dial face is covered as well as allowing for attachment to the watch case. To make sure a rigid outer rim is present as well as a rim that might later be used for assembly a rim with a width of 0.5 mm is created.

Inner Edge The inner size is mainly decided by visibility and precision. Since the design should indicate every second, the angle of the three mirrors combined is 6deg. On both sides of the flexure 10 μ is cut away for the gap. With the visibility limit being at 90 μm (see Section 3.1) and adding 10 μm to both sides, the inner flexure should have 110 μm space. With 180 flexures the minimum radius becomes 3.15 mm. To ensure visibility an inner radius of 3.5 mm is set. The inner edge is also set to have a minimum of 0.5 mm width. Placing the smallest radius at 3 mm.

Height To not exceed the height limit a maximum angle can be prescribed. The mirror plus a flexure should not exceed the 1 mm in height. Since there are 4 flexures and 3 mirrors, this angle varies based on their respective lengths as well as on the thickness of the mirror. The thickness of the wafer is 300 μm. Taking a flexure length of 0.87 mm and mirror length of 1.77 (the current dimensions) the maximum angle becomes 15.8deg. This angle can also be translated into an actuation displacement of 2.4 mm. These values do not take bending of the flexures into account, but it is a great initial guideline.

6.4 Flexure Stress

Now that the mechanical properties and dimensions of the mechanism are known, the flexure lengths can be minimized to maximize the mirror density. There are 2 types of flexures, the bending and the buckling flexures. Both were analyzed using the analytical Beam Constraint Model (BCM) in a 2D situation. Based on the results of the BCM a Finite Element Analysis (FEA) model was verified. The FEA model was then used to analyse the 3D mechanism.

Section 6.4.1 covers the Beam Constraint Model theory, which was applied to the bending and buckling flexures in Section 6.4.2. Section 6.4.3 analyzes the results of the BCM and these results were verified by a Finite Element Analysis in Section 6.4.4.

6.4.1 Beam Constraint Model

A great explanation of the Beam Constraint Model (BCM) is given in [97]. It is a well established analytical method for compliant flexures that undergo large deflections. A large deflection method is needed to analyze these flexures since nonlinear effects play a big role. The BCM uses a total of six variables: dx, dy and α to describe the position and orientation of the tip and takes the transverse force F, the axial load P and the moment M at the tip to define the loads. A schematic of the variables is given in Figure 37. If any three of these variables are known, the other three can be calculated using Equations 6 and 7,

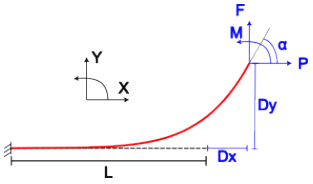

Figure 37: An illustration of the positive definitions of the BCM variables.

$$\begin{bmatrix} f \\ m \end{bmatrix} = (\bar{\bar{g}} + p\,\bar{\bar{p}} + p^2\,\bar{\bar{q}}) \begin{bmatrix} dy \\ \alpha \end{bmatrix}, \tag{6}$$

$$\begin{aligned} dx = &-\frac{1}{2} \begin{bmatrix} dy & \alpha \end{bmatrix} \bar{\bar{u}} \begin{bmatrix} dy \\ \alpha \end{bmatrix} \\ &- p \begin{bmatrix} dy & \alpha \end{bmatrix} \bar{\bar{v}} \begin{bmatrix} dy \\ \alpha \end{bmatrix} + \frac{t^2 p}{12L^2}, \end{aligned} \tag{7}$$

where the non-dimensional matrices have the values given in Equation 8,

$$\begin{aligned} \bar{\bar{g}} = \begin{bmatrix} 12 & -6 \\ -6 & 4 \end{bmatrix}, \quad \bar{\bar{p}} = \bar{\bar{u}} = \begin{bmatrix} 6/5 & -1/10 \\ -1/10 & 2/15 \end{bmatrix}, \\ \bar{\bar{q}} = \bar{\bar{v}} = \begin{bmatrix} -1/700 & 1/1400 \\ 1/1400 & -11/6300 \end{bmatrix}. \end{aligned} \tag{8}$$

The inertia and the normalized forces and sizes are defined by Equation 9,

$$\begin{aligned} I = \frac{wt^3}{12}, \quad m = \frac{ML}{EI}, \quad f = \frac{FL^2}{EI}, \quad p = \frac{PL^2}{EI}, \\ dy = \frac{Dy(L)}{L}, \quad dx = \frac{Dx(L)}{L}, \quad x = \frac{X}{L}, \end{aligned} \tag{9}$$

and the stress as function of x can be obtained using Equation 10,

$$\sigma_(x) = \sigma_b(x) + \sigma_t(x) = E\frac{u_y''(x)t}{2L} + E\frac{|P|}{A}, \tag{10}$$

where $u_y''(x)$ is defined by Equation 11,

$$u_y''(x) = \frac{\tan(r)\cos(rx) - \sin(rx)}{r} f + \frac{\cos(rx)}{\cos(r)} m, \tag{11}$$

with r = $\sqrt{-p}$, since the rattrapante force is compessive and thus negatively defined.

6.4.2 BCM applied to Bending and Buckling

How the BCM can be applied to the bending flexures is seen in Figure 38. For calculations, the flexure is split in two parts, and the connection between them is assumed to be a roller joint in Y-direction. The applied force of the rattrapante is purely axial and thus equal to P. Since the roller can not bear any transverse force, F will be zero. The moment M generated is directly related to the rattrapante force F_R, the mirror length L_m, thickness t_m and the angle α of the mirror. Since P and M are directly related we have 3 unknown variables F_R, Dx and Dy.

Using the same BCM equations, we can also describe the buckling flexure situation. This varies slightly from the bending flexure. Figure 39 shows the setup of the flexure. For this situation an extra variable is added: the moment exerted by the torsion hinge M_k. P is still equal to F_R. If the moment M = M_k, the transverse force F, which is not zero anymore, can be

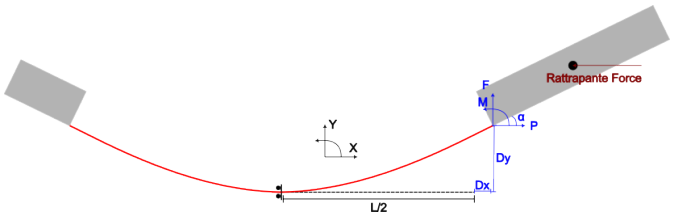

Figure 38: The BCM applied to the bending flexures.

describe by F = (P* h_y - M_k) / h_x where h_x and h_y are the distances from the rotation point to the flexure tip. Dy is directly related to the mirror orientation and geometry. This leaves us once again three unknowns: Dx, M_k and F_R.

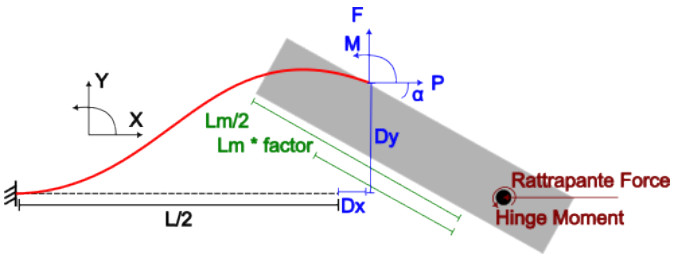

Figure 39: The BCM applied to the buckling flexures.

Please note that in this image, the connection point of the flexure is not at the end of the mirror. Buckling generates more stress, so the buckling flexure will take some of the length of the mirror. The extra benefit is that Dy will become smaller if the connection point is closer to the rotation point. This is also why the image shows L_m·factor. This factor determines the amount of length the mirror loses and the flexure gains.

6.4.3 BCM Results

For the bending flexures the maximum stress occurs at the roller joint, or halfway the flexure. A contour plot can be created for different mirror angles and flexure lengths. Please note that the length of the flexures influences the length of the mirrors as described in Section 6.3. The contour plot is shown in Figure 40a. For 3 mirrors, the angle will be somewhere around 15° to reach maximum height. Zooming in we can define the minimum length of the bending flexures. Figure 40b shows that a length of 0.46 mm is close to the 800 MPa limit and leaves some clearance for 3D effects. From the bending flexure length the mirror length can be calculated and set at 2.30 mm.

Using these values a buckling flexure contour can be created that uses the factor and the angle as variables. The contour is shown in Figure 40c. This contour also shows the maximum stress. For a buckling flexure, this maximum stress occurs at the inflection point closest to the mirror. The location of this inflection point changes position slightly for different angles, it is thus extracted by using a max() function. Figure 40d shows the stress as a function of the flexure length and the angle, zoomed in to the desired location of 15 °. (Notice that switching from 'factor of the mirror length added' to 'flexure length' flips the

(a)

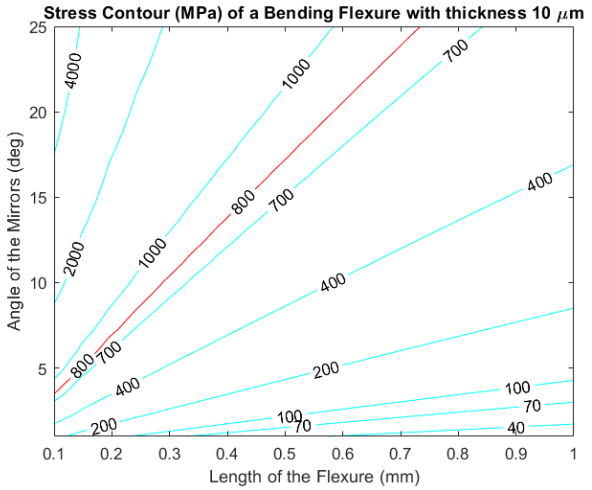

(b)

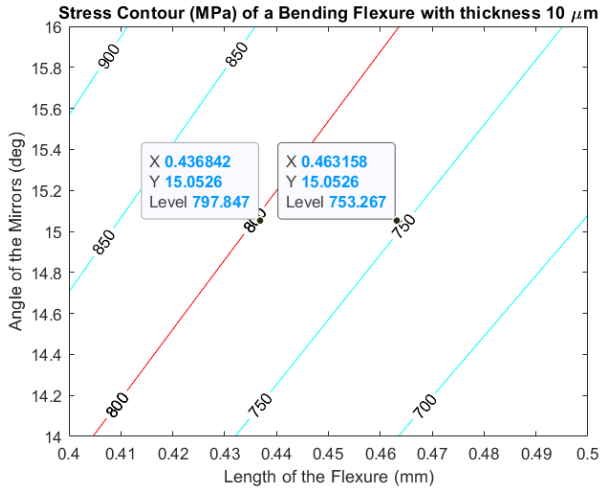

(c)

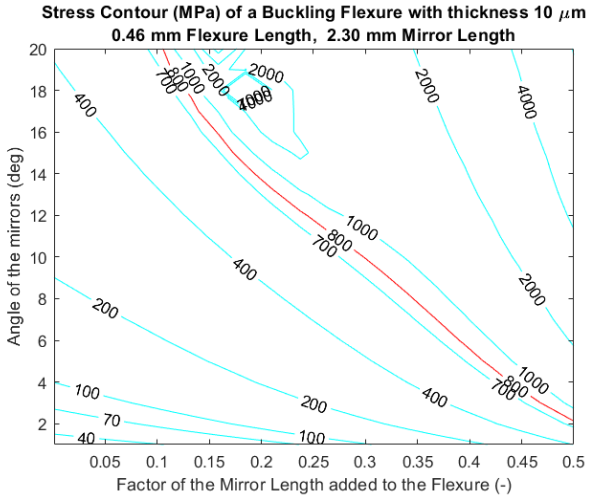

(d)

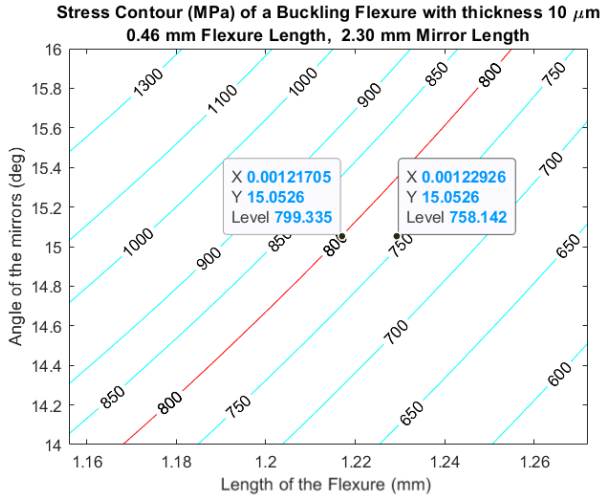

(e)

Figure 40: a) The full bending stress contour of angle vs. flexure length and b) the zoomed in contour around 15°.
c) The full buckling stress contour of angle vs. the factor added to the mirror and d) the zoomed in contour of angle vs. length. around 15°
e) The initial design (white) vs. the new design (anthracite) with the minimized flexure lengths to increase mirror density.

plot.) From this plot, once again leaving some clearance for 3D effects, a buckling flexure length of 1.23 mm is derived.

One will notice how there is a weird, non-continuous part for very big angles and specific factors is present in 40c. For large angles and displacements [97] describes the usage of the Chained Beam Constraint Model (CBCM). However, since the wrong stress results are not in the range of the desired flexure angle and the rest of the plot is continuous these results were still used.

The calculated values of 2.30 mm mirror length, 0.46 mm bending flexure length and 1.23 mm buckling flexure length were applied to the mirror and 3D printed. Figure 40e shows the new print in green and the initial design in white. From this image it is clear that by minimizing the flexure lengths, the mirror density increased.

6.4.4 Finite Element Analysis

This section will first validate Comsol® Finite Element Analysis (FEA) results. This was done before establishing definite values from the BCM method and thus uses dimensions of the white protoype in Figure 40e. After that, the values obtained from the BCM method will be analyzed by Comsol® to see the effects of the 3D structure. Most FEA Figures have a linear trafficlight color scheme between 750 and 850 MPa. Meaning that somewhere on the transition between yellow and orange the stress overshoots the stress limit.

Verify Comsol® and BCM To check if BCM corresponds to FEA results the dimesnions of the inital design were used. It has mirrors of 1.77 mm, bending flexures of 0.87 mm and buckling flexures of 1.53 mm. This buckling flexure gained a factor of 3/8 mirror length. The model is not shown, as the result looks (almost) exactly like the one in Figure 41a.

The model prescribes a 2.4 mm displacement of the inner boundary and it keeps the outer boundary fixed. Both the bending and buckling are validated. To achieve this 'line maximums' are implemented and derived by Comsol®. The lines are plotted at the zero-axis, thus in the middle of the flexures on the middle mirror row. This is where the 3D effects cancel each other out. For the bending flexures the line is plotted at the middle of the flexure and for the buckling flexure it is placed at $0.773 \cdot 1.53$ mm away from the outer edge. For these dimensions, this is where the maximum stress should occur according to the BCM. Table 5 summarizes the results. Seeing the small deviation between the two methods and the fact that Comsol® takes the diverging width of the flexure into account (even though small) the FEA is assumed to be valid and will be used for further analysis.

Table 5: The result of the BCM compared with the results of a FEA

	Angle (deg)	BCM Stress (MPa)	FEA Stress (MPA)	Error (%)
Bending Flexure	14.3	388	381	1.8
Buckling Flexure	14.7	396	380	4.2

3D effects Since both of these methods generate the same results, the dimensions obtained in Section 6.4.3 should be accurate. Importing the geometry with these dimensions and setting the displacement of the inner edge to 2.4 mm, the result in Figure 41a is obtained.

Both of the calculations were taken around the 750 MPa contour. The following two figures illustrate why some clearance was given for 3D effects. Figure 41b shows three bending flexures. One can clearly see that the outer flexures generate some extra moment on the middle flexure, which causes extra stress. The peak also occurs at the thinner end of the flexure, which is as expected. The stresses slightly overshoot the maximum allowable stress. However, the displacement (and thus the angle) will be lowered in Section 6.5.2 due to the hinge stresses, thus these dimensions will be held as final.

Figure 41c shows the stress in the buckling flexures. The figure shows that the buckling flexures shows little to no 3D effects. This is due to the fact that the outer boundary is constrained, and no rotation is possible there. So, once again, the BCM dimensions are used as final.

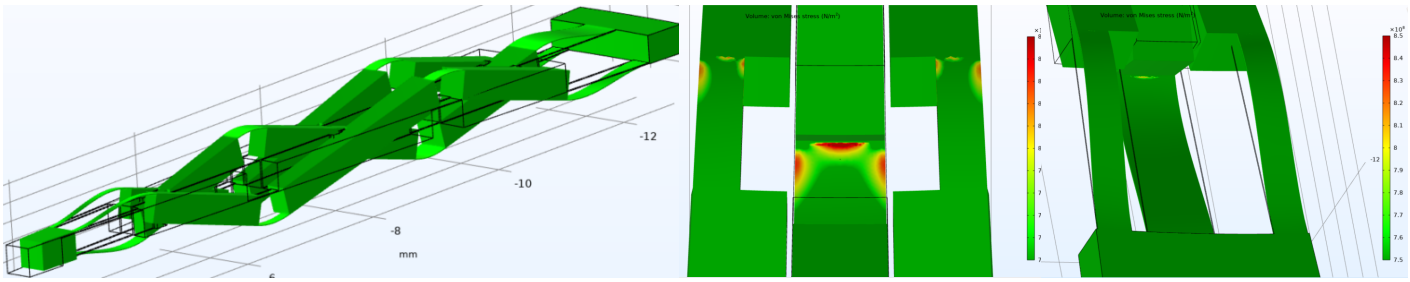

(a) (b) (c)

Figure 41: a) The actuated structure obtained from the FEA.
The stress obtained from the FEA in the b) bending and c) buckling flexures.

6.5 Torsion Hinge

As described in Section 6.2 the torsion hinge has to be redesigned to be produceable from two BOX layers. It still needs to constrain the mechanism to one degree of freedom however.

Section 6.5.1 will thus cover possible alternatives for the torsion hinge and Section 6.5.2 will tune the most feasible 'swan neck' hinge to fit the mechanism.

6.5.1 Hinge alternatives

A total of five possible hinges were created to constrain this mechanism. They will be covered one by one.

Off-Center The easiest way would be to simple move the hinge from the center to either the top or the bottom flexure as these can still constrain to pure rotation. They can either be all on the same level or they can alternate between the top and bottom. If all flexures are on the top (or bottom similarly) the 3D effects on the hinges create the bending shown in Figure 42. This is undesirable due to the fact that pieces of mirror would have to be removed to allow for these rotations.

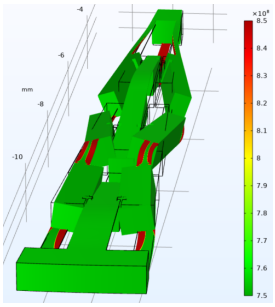

Figure 42: The result of moving the torsion hinges to the top layer.

If the flexures alternate between high and low the bending in Figure 44 is realized (this hinge has two high hinges and one low hinge). This asymmetric upward bending does not have to be a problem. For a square beam, 10x10 μm, the height reached is 0.59 mm, which is within the design space. However, the hinge itself experiences to much stress, as can be seen in Figure 43. The maximum stress is evaluated at 7.7 GPa, which is a factor 10 to high for the allowable stress. Varying the width of the hinge to 20x10 or 5x10 μm changes the stress to 10.2 and 7.1 GPa respectively. This hinge will thus not become feasible, irrespective of its dimensions. The difference between two high hinges and 2 low hinges yield approximately the same stresses and displacements, only toward the bottom instead of the top.

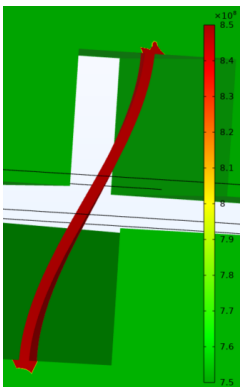

Figure 43: An off-center torsion hinge experiences to much stress.

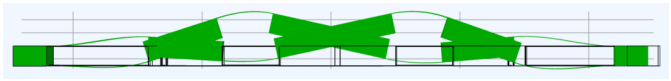

Figure 44: The asymmetric deformation for alternating high and low off-center hinges.

4 Beams One could also use two intersecting plane constraints to get one rotational DoF [98]. Two beams can create a plane constraint. Thus placing four beams as shown in Figure 45a, one can constrain to only rotation around the red arrow. By evaluating this hinge with FEA, see Figure 45b, one can clearly see why this hinge does not work. The rotation generates a displacement as well as a rotation of the beams. The stress due to this is simply to high.

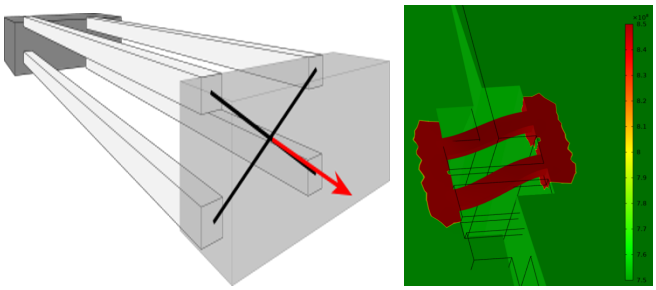

(a) (b)

Figure 45: a) The theory of constraining to rotation (red arrow) by using two constraining planes (black) and b) the resulting stress of such a hinge.

Separate Mirror Pieces A sub-optimal but possible solution would be to split the mirrors in half, add a 'ring' in gaps (added only for this purpose) and glue them together. This would look like the schematic shown in Figure 46. The ring can then act as a physical stop. This solution is not desired since once split, a mechanism to indicate 1 second would become 12 separate pieces. This will make assembly very hard if not impossible, but is might be a solution if everything else fails.

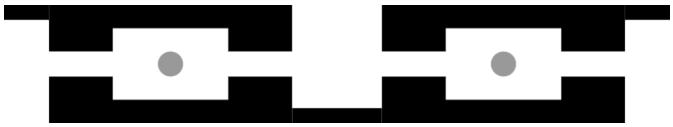

Figure 46: An illustration of how the mirrors would be split and the placement of the constraining rings.

Physical Stop A fourth possibility would be to utilize a physical stop. Figure 47 shows the structure that would be used. By mirroring the structure on the other mirror and interlocking, both of overhanging beams can move downward through the red BOX layer until it touches the main mirror. A contour plot of the needed BOX layer thickness was created as a function of the width of the overhanging beam and the angle of rotation desired. It is shown in Figure 48. BOX layer thickness can vary between 500 nm and 2 μm [84, p.208], those values are indicated as red lines

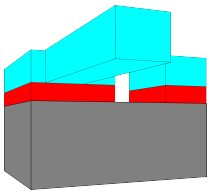

Figure 47: An illustration of the physical stop hinge.

in the plot. It is clear that this is not a feasible solution for the angles these mirrors need to achieve.

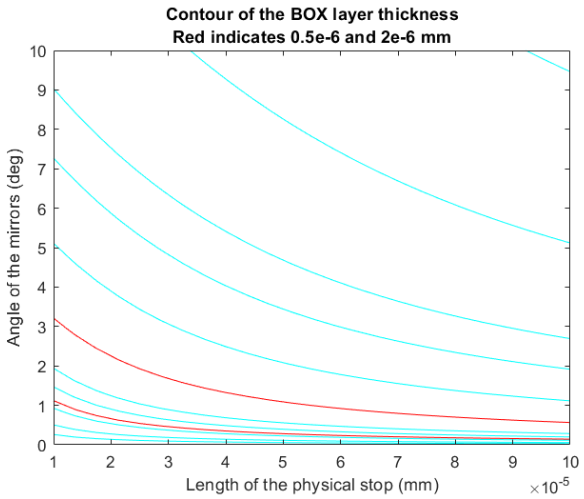

Figure 48: The contour plot of the BOX layer thickness required as a function of the mirror angle and physical stop width.

Swan Neck The last solution is a 'swan neck' hinge. It is connected to the top of the mirror on one side and connected to the bottom side of the other. It is a combination of the standard torsion hinge and the off-center hinge. An evaluation with FEA is shown in Figure 49. The maximum stress in the hinge is 2.35 GPa, this is slightly to high, but much closer to the 800 MPa limit than for example the off-center hinge. This is due to the fact that the beam connected the high and low parts of the hinge can take some torsional stress by buckling itself.

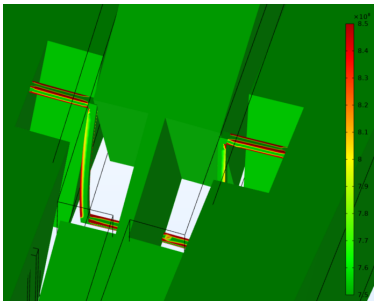

Figure 49: The stress in the 'swan neck' hinge.

Hinge Choice So, from the five described possibilities that constrain the system only the 'separate pieces' and 'swan neck' might be feasible. Since the separate pieces is not a compliant hinge and assembly is hard, it will be discarded. This leaves the 'swan neck', which will have to be explored more in depth to tune the dimensions.

6.5.2 Swan Neck

As stated, the swan neck hinge has to be tuned to get the stress within the 800 MPa limit. To tune these hinges quite some parameters can be changed. This section will highlight the variables that were changed.

Displacement The displacement of at the center of the mirror is a main parameter that changes the stress in the flexures and hinges. The displacement is reduced from 0.24 to 0.16 mm. This reduction has three effects. First and foremost, it reduces the stress in the swan neck from 2.35 to 1.57 GPa. This should make tuning the hinge to the 800 MPa limit more reachable. Secondly, it reduces the stress in the bending and buckling flexures. As explained in Section Section 6.4.4, this stress was slightly higher than calculated by the Beam Constraint Model due to 3D effects. Lowering the displacement removes the problem areas shown in Figure 41b. Thirdly, it changes the angle of the mirrors, this is not a positive effect, however, the angle of the mirrors is reduced to 13° from 15°, so it is assumed not significant for the visual effect itself. The first two arguments also outweigh the negative third argument.

High-Low Flip The hinges all have a high and a low connection to the mirrors. These connections alternate with respect to the previous hinge. Currently, the middle hinge is connected high to the center mirrors. If one changes this to a low connection, and thus flipping all the hinge connections from high to low and vice versa, the 3D effects change the stress. For a high connection the stress currently is 1.57 MPa, for a low connection, this is reduced to 1.39 GPa. This change occurs due to a combination of two factors. The flexure above a hinge is stronger than the one below it + the flexures on the side generate a moment on the hinge that is bigger than the moment generated by the flexures in the middle due to their position. By flipping the connections, these two factors generate less stress.

Double Swan Another option that was tried to reduce the stress was to create a hinge that goes up and down an extra time. Figure 50 shows the deflection of this 'Double Swan' hinge. Even though it does fit geometrically (it does not touch itself), it increases the maximum stress to 6.58 GPa. It is thus not an improvement and discarded.

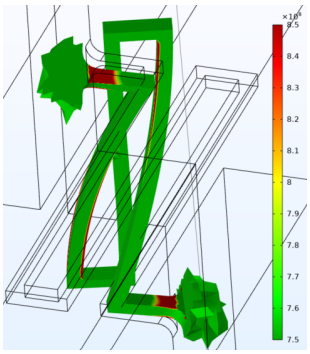

Figure 50: The deflection of a 'Double Swan' Hinge.

Upper Flexure Position Due to the asymmetry in between the middle and side flexures and the moment they generate, the placement of the upper buckling flexure (the strongest) might have influence on the stress. This was analyzed by moving this flexure slightly inward, as shown in Figure 52a. The maximum stress however, increases from 1.39 to 2.38 GPa. Thus, this change is not positive and is discarded.

Due to an error, this was assumed to be a positive change. This is the reason why the demonstrator, in Section 7 is printed with these flexures moved.

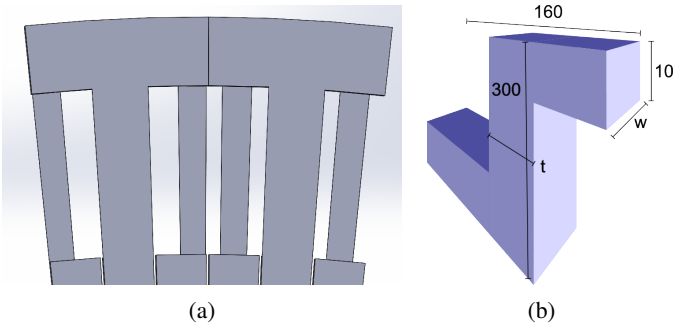

(a) (b)

Figure 52: a) The placement of the current (left) vs. moved (right) upper flexures and b) a schematic drawing of the dimensions and tunable parameters of the swan neck.

Hinge Dimensions The stress is already reduced from 2.35 to 1.39 GPa, however, the hinge itself can also still be tuned. A schematic of the hinge is shown in Figure 52b, which shows that the hinge itself has two tunable dimensions. The width of the flexure 'w' and the thickness of the middle beam 't'. The length of the flexure 'L' is fixed at 160 μm, if this length is longer the inner hinge passes through the mirror as shown in Figure 40e. The heights of 300 μm and 10μm are already determined by the wafer thickness and BOX-layer position respectively.

A small parametric sweep was performed to check the influence of these parameters. Table 6 shows the stresses derived for all three of the hinges separately. Figures 51a, 51b and 51c show how the hinge deflection changes for beams of 5, 10 and 20 μm respectively. These Figures are included to give the reader a feeling for the bending of the middle beam and thereby for the values given in the Table.

To keep the maximum stress as low as possible it was chosen to set the t and w both to 10 μm. Even though the 1.39 GPa overshoots the 800 MPa It is clear from Figure 51b that the maximum stress occurs in compression. As stated in Section 6.2, silicon is a brittle material and compressive stress can breach this limit and this exceedance is thus accepted.

Table 6: The stresses in all 3 hinges as a function of the width and thickness of the hinge.

Dimensions (μm)		Stresses (GPa)		
t	w	H1	H2	H3
5	5	0.74	1.30	3.10
5	10	0.84	1.30	1.53
10	5	0.81	1.15	2.43
10	10	0.85	1.18	1.39
10	20	1.38	1.46	1.61
20	10	1.06	1.17	1.80
20	20	1.95	1.94	2.02

6.6 Actuation

The mechanism needs to be actuated consistently. This section covers the actuation from the force conversion to the colum wheel.

The original Mechanical Mirrors were conceptualized using a vertical clutch. However, the final design needs a horizontal force. To achieve this force there are two possibilities. Either generate a horizontal force or convert the vertical force into a horizontal one. To generate a horizontal force the rattrapante axis should allow for rotation as well as horizontal displacement. This horizontal displacement would need some kind of flexible axis. This seems overly difficult. Thus, the vertical force from the clutch will simply be converted into a horizontal one. This is achieved by creating an extension on the rattrapante gear. This extension consists of a triangle followed by an overhanging arm as shown in Figure 53c. If the rattrapante gear moves down, an angled force will be exerted on the desired section. If the mirrors are constrained in the vertical direction, the mechanism will be subject to a horizontal force only. The overhanging arm is there to possibly constrain rotation of the inner edge.

The vertical clutch is actually a 'discrete vertical clutch gripper'. It needs to move the rattrapante gear vertically as well as grip it in discrete steps to ensure that only one mirror is actuated. A couple of things happen at the same time. By activating

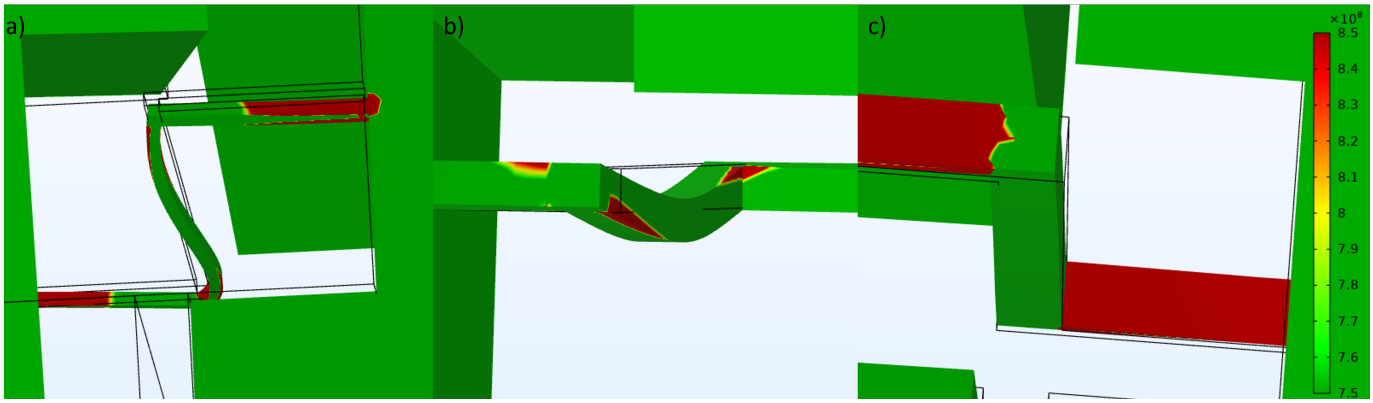

Figure 51: The difference between bending of the hinges when the width and thickness are a) 5x5 μm, b) 10x10 μm and c) 20x20 μm.

a column wheel the 2 arms of the gripper move in and outward. This column wheel is shown in Figure 53a. It consists of 8 columns and 16 ratchets to ensure that the arms either are or are not gripping the system for every ratchet activation. How column wheels work for rattrapantes in also explained in [48].

If the arms fall between the column wheel pillars, they move toward each other to grip the rattrapante gear. The vertical displacement is achieved by ridges that have a small angle, and push the gear down. This is designed with [44] as inspiration. At the end of that ridge there are indents in the arm. These indents match the teeth of the rattrapante gear and are shown in Figure 53b. There are 60 teeth in total to match the 60 sections of the mechanism. These indents ensure the discrete gripping of the gear. The entire actuation mechanism is shown in Figure 53d.

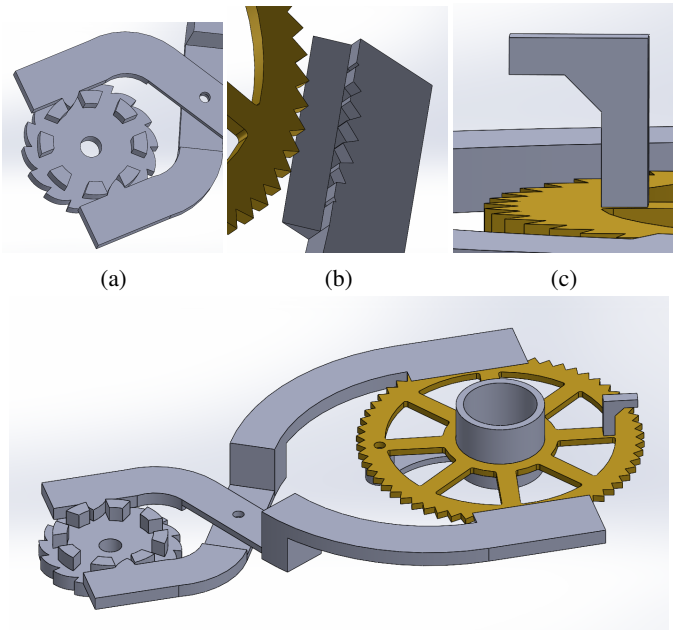

(a) (b) (c)

(d)

Figure 53: a) The column wheel which activates b) the discrete vertical clutch gripper. c) The extension that convert the vertical force to a horizontal one and d) an overview of how these parts connect to each other.

6.7 Geometric fit

With the actuation designed the entirety of the mechanism has to be fit into the design space. Since the column wheel has quite some height it is placed in the chronograph space. The chronograph wheel and the heart are also in the chronograph space. The grippers start at the column wheel, and after their hinge point they have a vertical beam to rise to the rattrapante wheel, this can also be seen in Figure 53d.

The mirrors are exactly halfway the 1 mm height, leaving 0.35 mm between the mirrors and the chronograph. Just below the mirrors is a 'force ring', shown in Figure 54. It ensures that the vertical force of the vertical clutch is cancelled and the mirrors can only move outward. This force ring is connected by 5 tubes to the plate. Between these mirrors the grippers fit with a 0.01 mm tolerance on both sides.

The rattrapante gear has a radius of 2.5 mm. This size was chosen to reduce the inertia. The force conversion has to be connected to the gear and the grippers can not touch this extrusion. This means the mirrors have to be smaller than the current 3.0 mm radius to allow the extrusion to actuate the mirrors. The inner radius of the mirrors is changed to 2 mm.

The view from the bottom is shown in Figure 54 where the force ring is shown in blue and the chronograph gear is hidden. One can also see the spring against the heart shape to return the rattrapante.

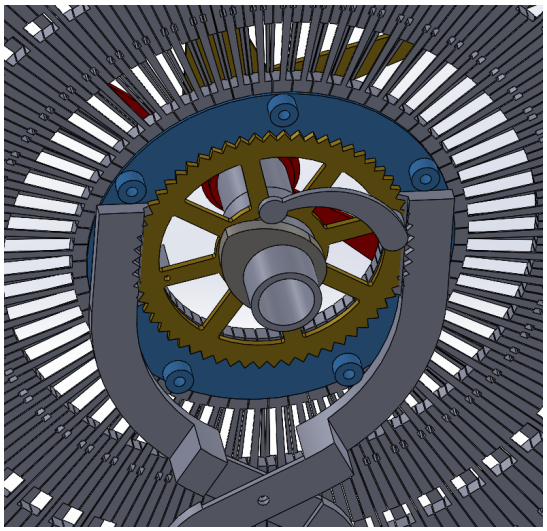

Figure 54: A bottom view of the mechanism with the force ring highlighted in blue.

Since there is no constraint on top of the mirrors, it needs to be checked if the influence of gravity moves the mirrors. Once again, using FEA the total displacement of the mirrors is evaluated at 37 nm. It is thus negligible with respect to the clearance with the force conversion extension.

7 Results

To demonstrate how and that this mechanism worked as well as how the visual effect behaved the entire mechanism was produced and build at scale. An actual size model would require a master watchmaker and was not in the scope of this research.

The mirrors for the demonstrator were produced using a 3D printer with black PET-G. Since the printer has a layer thickness of 0.15 mm combined with a flexure thickness is 0.01 mm a scale of 15:1 was chosen. This makes the flexures exactly one layer thick. After some testing, it became clear that single layer

(a)

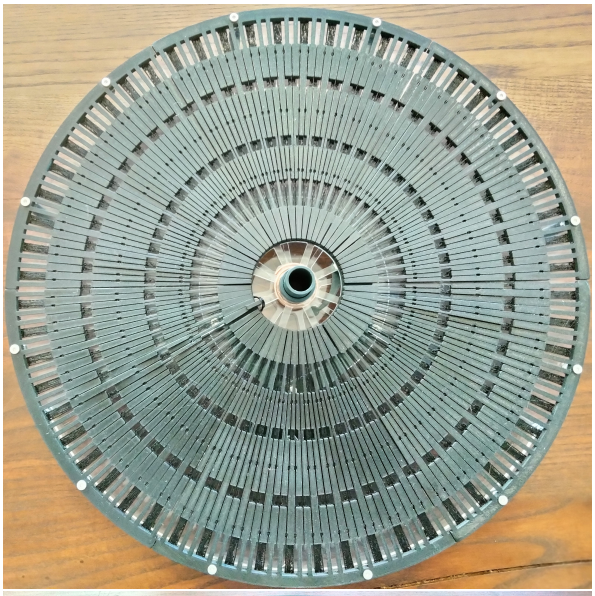

(b)

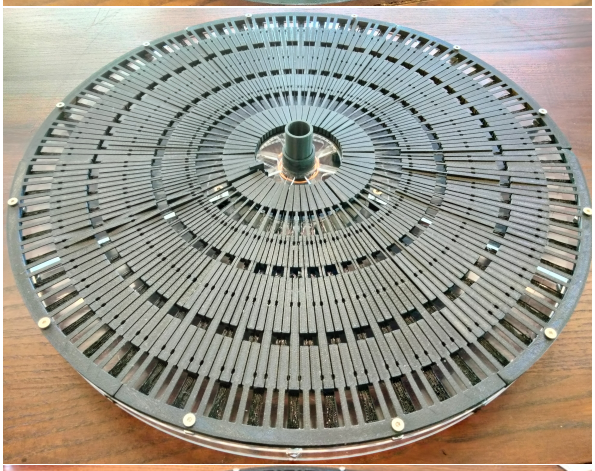

(c)

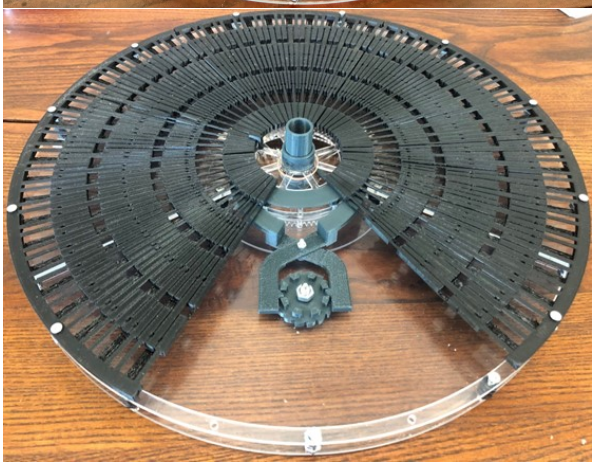

Figure 55: The demonstrator from the a) top, b) from a 45° angle and c) with some mirrors removed to highlight the actuation.

flexures printed on top of supports break if one wants to remove the supports. Thus it was decided that the flexures would be printed with a thickness off 2 layers. The increase of stress in the mirrors due to thicker flexures does not matter since PET-G is more flexible than silicon. The swan neck hinge is not printable by this 3D printer since it stacks single 'dots' on top of each other, which then fall over during printing. The demonstrator was thus printed with the initial torsion hinge.

(a)

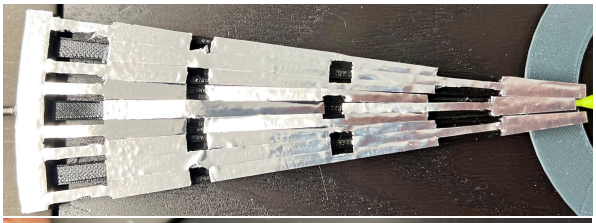

(b)

Figure 56: Actuated mirrors covered with aluminum tape to show how the effect looks with refelction in the a) top and b) isometric view.

To assemble the mirrors and the actuation parts (also 3D-printed) the bottom of the rattrapante and the chronograph were lasercut from 4mm acrylic sheets. Assembling everything yielded the demonstrator in the following figures. Figures 55a and 55b show the demonstrator from the top and from a 45° angle respectively. Both with one mirror actuated. Figure 55c shows the demonstrator with some mirrors removed to highlight the position of the actuation. One will also notice that these mirrors were printed with the 'moved upper flexure' from Section 6.5.2. The mistake of assuming this 'moved upper flexure' reduces the stress was discovered when the 3D-printer had already ran for 50 hours straight, and for money, time and environmental reasons it was decided to not reprint all these parts. Since the mirrors were printed in black the visual effect is harder to see due to very little reflection and contrast. A set of 3 mirrors was covered in aluminum tape to achieve the desired reflection. They are shown in Figure 56 from the top and in isometric view.

8 Conclusion and Discussion

This thesis has completed a full design cycle to deliver a new way to visually indicate time in a rattrapante complication of a mechanical watch.

According to the aesthetic survey conducted this is an aesthetically pleasing idea and it also fits the design space for this mechanism. Since the needle indicator is left out in this design, and only a heart and rattrapante gear are present, this design will not influence the runtime of the watch as much as a normal rattrapante complication. The smallest length in this design is exactly the visibility limit for normal human acuity. However, since all parts are diverging towards the outer edge, most people will be able to read out the indicator when wearing this watch. Wearing this mechanism in a watch should not break the mechanism nor should it break from shocks applied to it, since the mirrors are compliant and can thus bend without breaking.

As of today, no patent has been found which comes anywhere near this design, making it novel in the watchmaking world. This design is more difficult to assemble than a standard rattrapante due to the force ring under the tip of the mirrors. It should however be assemblable in approximately the same way as a normal rattrapante. Even though it is hard to produce by using 3D printers on a 15:1 scale, this design can, theoretically, be produced from a double BOX-layered silicon wafer, allowing it to be produced with a high accuracy and repeatability.

Although this thesis designed a feasible visual effect to replace the needle indicator of a rattrapante complication some critical notes have to be placed.

As a very first. The only thing that does not satisfy the boundaries set is the swan neck torsion hinge. It exceeds the stress limit of 800 MPa. It was already stated twice that compressive stress can be higher than tensile stress and that the stress in the swan neck stress in to high in compression and in combination with the difference in reported stress limits it will probably be fine. However, due to the nature of silicon wafer production, the surface cracks present in wafers and the low thickness of the hinge it could be that this hinge fails due to one unluckily placed crack. This is currently not testable however, and will have to be experienced after production.

A second note can be placed on the relevance of this design as a rattrapante complication. The rattrapante complication is almost the epitome of luxury watchmaking, if I ever get to see and hold one, let alone own one, I would be a very lucky man. The fact that it is such a luxury item brings two things to the table: the relevance as well as the customer base.

This mechanism of course can be sold as an luxury item, but it might also be used to revolutionize the indicators we use everyday. Changing all indicators all at once might be a step to far, but starting with for example using it as a minute indicator could be very feasible. The minute hand travels 60 times as slow, making friction and inertia a much smaller problem. It might thus be used as a continuous, instead of an on demand, mechanism. Actuation could be as simple as rotating a cam in the center of the mirrors instead of the minute hand. This cam could actuate the mirrors one by one, and transitions to the next minute could happen smoothly. Using it as a minute indicator will increase the amount of times it can be used in a watch (mechanical or quartz) for a much lower price tag, and thus increase it's daily occurrence and relevance.

With respect to the customer base: this visual effect was assessed as aesthetically pleasing by a group that does not represent the customer base for rattrapante complications. Which, and I am sorry if I step on the wrong foot here, will in general consist of wealthy males. Even though a lot of participants were male, none of them were rich. Also, a significant enough amount of the control group was female, allowing it to be assessed as unisex. This might, due to the assumed customer base, not be the best way to make this idea sell well. Once again, one can conclude that this design might be better fit as a minute indicator on more accessible watches.

Acknowledgements

I want to thank Flexous Mechanisms for allowing me to do my thesis project at their company and supplying me with resources, materials and machines. With special regard to G. Dunning and A. Yellowhorse for guiding me in this research in the name of the Company. I also want to thank H. Goosen as my TU Delft supervisor for his insights in mechanical systems, I was always satisfied with our conversations. As last, but not least, I want to thank to A. Elbakyan for her continued fight in making science accessible to everyone.

References

[1] G. A. Kern, "Engineering the intangible: Strategic success factors in the luxury watch industry," in *Evolving Business Models*. Springer, 2017, pp. 153–180.

[2] B. Ciechanowski, "Mechanical watch," Ciechanow.ski, accessed Nov. 4, 2022. [Online]. Available: https://ciechanow.ski/mechanical-watch/

[3] L. T. White and L. White, *Medieval technology and social change*. Galaxy Books, 1964, vol. 163.

[4] K. Damasko, "Mechanical winding mechanism for wrist watches and a wrist watch with such a winding mechanism," Patent EP Patent 199,823,5A2, May 30, 2088. [Online]. Available: https://patents.google.com/patent/EP1998235A2/en

[5] "Famous watchmakers," Haute Horlogerie, accessed Nov. 4, 2022. [Online]. Available: https://web.archive.org/web/20081208011657/http://www.hautehorlogerie.org/en/players/famous-watchmakers/18th-century/abraham-louis-breguet.html

[6] "Triple axis tourbillon regulator," Thomas Prescher, accessed Nov. 4, 2022. [Online]. Available: https://www.prescher.ch/triple-axis-tourbillon-regulator

[7] K. Uchida, "World clock," Patent US Patent 4,779,247, Oct. 18, 1988. [Online]. Available: https://patents.google.com/patent/US4779247A/en

[8] "Calendar function," A.Lange & Söhne, accessed Nov. 4, 2022. [Online]. Available: https://www.alange-soehne.com/eu-en/timepieces/selections/calendar-watches

[9] M. Wallace, "Clock movement with moon dial," Patent US Patent App. 10/699,171, May 5, 2005. [Online]. Available: https://patents.google.com/patent/US20050094491A1/en

[10] O. Müller, "Louis moinet," World Tempus, accessed Nov. 6, 2022. [Online]. Available: https://en.worldtempus.com/article/industry-news/brands/louis-moinet-the-first-ever-chronograph-14459.html

[11] E. Doerr, "Richard habring's personal iwc portugieser split-seconds chronograph prototype ref. 3712 at phillips geneva watch auction xii: A unique piece of horological history," Quill & Pad, accessed Nov. 11, 2022. [Online]. Available: https://quillandpad.com/2021/05/01/richard-habrings-personal-iwc-portugieser-split-seconds-chronograph-prototype/

[12] T. L. Martin, "Time and time again: Parallels in the development of the watch and the wearable computer," in *Proceedings. Sixth International Symposium on Wearable Computers,*. IEEE, 2002, pp. 5–11.

[13] "The patented zero-reset," A. Lange & Söhne, accessed Nov. 4, 2022. [Online]. Available: https://www.alange-soehne.com/gb-en/manufactory/art-of-watchmaking/zero-reset-mechanism
[14] "Precision," COSC, accessed Nov. 6, 2022. [Online]. Available: https://www.cosc.swiss/en/quality/precision
[15] "Quartz movements," COSC, accessed Nov. 6, 2022. [Online]. Available: https://www.cosc.swiss/en/certification/quartz-movements
[16] M. Rikitianskaia and G. Balbi, "What time is it? history and typology of time signals from the telegraph to the digital," *International Journal of Communication*, vol. 15, p. 18, 2021.
[17] A. M. Cohen, "The clockwork self and the horological revolution," in *Shakespeare and Technology*. Springer, 2006, pp. 127–149.
[18] W. F. Grether, "Instrument reading: The design of long-scale indicators for speed and accuracy of quantitative readings." *Journal of Applied Psychology*, vol. 33, no. 4, p. 363, 1949.
[19] R. B. Sleight, "The effect of instrument dial shape on legibility." *Journal of Applied Psychology*, vol. 32, no. 2, p. 170, 1948.
[20] D. Conradie, "Mechanical 7-segment display uses a single motor," Hackaday, accessed Nov. 7, 2022. [Online]. Available: https://hackaday.com/2021/06/27/mechanical-7-segment-display-uses-a-single-motor/
[21] Shiura, "3d printed mechanical digital clock," Youtube, accessed Nov. 7, 2022. [Online]. Available: https://www.youtube.com/watch?v=vqSXs7R05LQ
[22] M. Robin, "Character display mechanism for a timepiece," Patent US Patent 9,436,160, Sep. 6, 2016. [Online]. Available: https://patents.google.com/patent/US9436160B2/en
[23] F. Quentin, "Device for displaying the time in digital form in a timepiece having a mechanical movement," Patent EP Patent 244,352,4B1, Aug. 14, 2013. [Online]. Available: https://patents.google.com/patent/EP2443524B1/en
[24] N. Mitamura, "Timepiece," Patent US Patent 11,137,722, Oct. 5, 2021. [Online]. Available: https://patents.google.com/patent/US20190086870A1/en
[25] C. Claret, J. Dubois, A. Schiesser, and F. Gruosi, "Timepiece provided with open dial plate," Patent US Patent 7,420,885, Sep. 2, 2008. [Online]. Available: https://patents.google.com/patent/US7420885B2/en
[26] J.-M. Wiederrecht and R. Gil, "Retrograde sector display device," Patent EP Patent 110,213,4A1, May 23, 2011. [Online]. Available: https://patents.google.com/patent/EP1102134A1/en
[27] R. Courvoisier, E. Roman, and P. Bravo, "Multi-sector display," Patent US Patent 8,717,853, May 6, 2014. [Online]. Available: https://patents.google.com/patent/US20120067271A1/en
[28] J. Choksi and D. Zimmermann, "Linear time display," Patent US Patent App. 11/514,104, Mar. 29, 2007. [Online]. Available: https://patents.google.com/patent/US20070070819A1/en
[29] F. Brandenburg, "Time display mechanism," Patent EP Patent 141,633,9B1, May 27, 2009. [Online]. Available: https://patents.google.com/patent/EP1416339B1/en
[30] S. Perret and L. Vouillamoz, "Detail of a wrist watch," Patent US Patent App. 29/516,961, Feb. 28, 2017. [Online]. Available: https://patents.google.com/patent/USD779987S1/en
[31] S. J. Mueller, "Position indicator, measuring apparatus and method of manufacturing a position indicator," Patent US Patent 7,502,280, Mar. 10, 2009. [Online]. Available: https://patents.google.com/patent/US7502280B2/en
[32] M. Yuichi, "Display mechanism, watch movement and watch," Patent JP Patent 633,409,8B2, May 30, 2018. [Online]. Available: https://patents.google.com/patent/JP6334098B2/en
[33] J.-M. Wiederrecht and P. Junod, "Timepiece movement for driving a display element along a complex path and timepiece comprising such a movement," Patent US Patent 7,969,824, Jun. 28, 2011. [Online]. Available: https://patents.google.com/patent/US7969824B2/en
[34] M. Stranczl, "Flexible resilient hand," Patent US Patent 9,075,392, Jul. 7, 2015. [Online]. Available: https://patents.google.com/patent/US9075392B2/en
[35] H. Jolidon, "Timepiece with variable hour circle," Patent US Patent 8,199,612, Jun. 12, 2012. [Online]. Available: https://patents.google.com/patent/US8199612B2/en
[36] F. Baumgartner and M. Frei, "Timepiece with mechanism indicating a period of time," Patent EP Patent 170,553,5B1, Jul. 11, 2007. [Online]. Available: https://patents.google.com/patent/EP1705535B1/en
[37] G. Fonseca, "Timepiece movement provided with a rotary, hollow, three-dimensional element," Patent EP Patent 273,592,0A2, Mar. 18, 2020. [Online]. Available: https://patents.google.com/patent/EP2735920A2/en
[38] M. Buttet, E. Barbasini, and M. Navas, "Mechanism for displaying figures or signs produced on a timepiece dial," Patent US Patent 7,839,727, Nov. 23, 2010. [Online]. Available: https://patents.google.com/patent/US7839727B2/en
[39] ——, "Mechanism for displaying pictures, figures or signs produced on a timepiece dial," Patent US Patent 7,821,879, Oct. 26, 2010. [Online]. Available: https://patents.google.com/patent/US7821879B2/en
[40] D. Nebel, "Display mechanism for a timepiece of a wrist watch," Patent EP Patent 353,422,3A1, Mar. 01, 2019. [Online]. Available: https://patents.google.com/patent/EP3534223A1/en
[41] E. Goeller and A. Zaugg, "Astronomical watch," Patent US Patent 8,995,233, Mar. 31, 2015. [Online]. Available: https://patents.google.com/patent/US8995233B2/en
[42] C.-A. Reymondin, G. Monnier, D. Jeanneret, U. Pelaratti, and E. technique de la Vallée de Joux (Le Sentier), *The theory of horology*. Swiss Federation of Technical Colleges: Watchmakers of Switzerland, Training and Educational Program Neuchâtel, 1999.
[43] O. Mertenat, "Column-wheel for a chronograph, chronograph and chronograph watch including such a wheel," Sep. 10 2013. [Online]. Available: https://patents.google.com/patent/US8529121B2/en
[44] K.-F. Scheufele, "Vertical clutch device for timepiece," Patent US Patent 7,712,953, May 11, 2010. [Online]. Available: https://patents.google.com/patent/US7712953B2/en
[45] A. Kruttli and D. Chabloz, "Device for a timepiece," Patent US Patent 10,496,039, Dec. 3, 2019. [Online]. Available: https://patents.google.com/patent/US10496039B2/en
[46] L. Perret and S. Forsey, "Time piece chronograph clockwork movement," Patent US Patent 7,597,471, Oct. 6, 2009. [Online]. Available: https://patents.google.com/patent/US7597471B2/en
[47] T. Philippine, "Split-seconds device with epicycloidal train for a timepiece," Patent EP Patent 302,117,5B1, May 18, 2016. [Online]. Available: https://patents.google.com/patent/EP3021175B1/en
[48] W. . Co., "How on earth does a split-second chronograph work? — watchfinder & co." Youtube, accessed Nov. 20,

2022. [Online]. Available: https://www.youtube.com/watch?v=ozK6NFb2Ya4

[49] Y. Pintus, M. Pintus, and J.-L. Perrin, "Retrograde chronograph mechanism with rattrapante hand," Patent EP Patent 311,295,6B1, Aug. 22, 2018. [Online]. Available: https://patents.google.com/patent/EP3112956B1/en

[50] P. Brida, D. Zimmermann, and S. Ihnen, "Watch with fly back hand function and corresponding fly back hand mechanism," Oct. 31 2006. [Online]. Available: https://patents.google.com/patent/US7130247B2/en

[51] "The development of the rattrapante function," A. Lange & Söhne, accessed Nov. 11, 2022. [Online]. Available: https://www.alange-soehne.com/ww-en/manufactory/art-of-watchmaking/rattrapante-mechanism

[52] WatchTime, "Splendid splitters: 5 noteworthy rattrapante chronograph watches," WatchTime, accessed Jun. 08, 2023. [Online]. Available: https://web.archive.org/web/20230329130924/https://www.watchtime.com/featured/splendid-splitters-5-noteworthy-rattrapante-chronograph-watches/

[53] S. Albert, "Measuring aesthetic value," Arts Proffesional, accessed Nov. 7, 2022. [Online]. Available: https://www.artsprofessional.co.uk/magazine/298/feature/measuring-aesthetic-value

[54] J. Shelley, "The concept of the aesthetic," Stanford Encyclopedia of Philosophy, accessed Nov. 7, 2022. [Online]. Available: https://plato.stanford.edu/entries/aesthetic-concept/

[55] A. A. Brielmann and D. G. Pelli, "Aesthetics," *Current Biology*, vol. 28, no. 16, pp. R859–R863, 2018.

[56] K. T. Ulrich, *Design: Creation of Artifacts in Society*, 2011, ch. Aesthetics in design.

[57] S.-W. Hsiao, F.-Y. Chiu, and C. S. Chen, "Applying aesthetics measurement to product design," *International Journal of Industrial Ergonomics*, vol. 38, no. 11-12, pp. 910–920, 2008.

[58] A. Haug, "A framework for the experience of product aesthetics," *The design journal*, vol. 19, no. 5, pp. 809–826, 2016.

[59] A. H. Goldman, *Aesthetic value*. Routledge, 2018.

[60] M. R. Goode, D. W. Dahl, and C. P. Moreau, "Innovation aesthetics: The relationship between category cues, categorization certainty, and newness perceptions," *Journal of Product Innovation Management*, vol. 30, no. 2, pp. 192–208, 2013.

[61] J. Han, H. Forbes, and D. Schaefer, "An exploration of how creativity, functionality, and aesthetics are related in design," *Research in Engineering Design*, vol. 32, no. 3, pp. 289–307, 2021.

[62] P. Hekkert, "Design aesthetics: principles of pleasure in design," *Psychology science*, vol. 48, no. 2, p. 157, 2006.

[63] C. CHUNG, "Time, culture and identity: Exploring horological collections with uk-china museum audiences," *Chinese Annals of History of Science and Technology*, vol. 4, p. 82, 2020.

[64] P. S. Jitender, "Understanding the relationship between aesthetics and product design," *International Journal of Engineering Technology Science and Research*, vol. 5, no. 3, p. 6, 2018.

[65] J. E. Sheedy, I. L. Bailey, and T. W. Raasch, "Visual acuity and chart luminance." *American journal of optometry and physiological optics*, vol. 61, no. 9, pp. 595–600, 1984.

[66] "Visual acuity of the human eye," Iowa State University, accessed Nov. 7, 2022. [Online]. Available: https://www.nde-ed.org/NDETechniques/PenetrantTest/Introduction/visualacuity.xhtml

[67] J. Gordon and B. Clark, "Analogue and digital time displays for military wristwatches." AERONAUTICAL RESEARCH LABS MELBOURNE (AUSTRALIA), Tech. Rep., 1982.

[68] B. Inditsky, H. Bodmann, and H. Fleck, "Elements of visual performance: contrast metric—visibility lobes—eye movements," *Lighting Research & Technology*, vol. 14, no. 4, pp. 218–231, 1982.

[69] H. R. Blackwell and O. M. Blackwell, "Population data for 140 normal 20–30 year olds for use in assessing some effects of lighting upon visual performance," *Journal of the Illuminating Engineering Society*, vol. 9, no. 3, pp. 158–174, 1980.

[70] W. Meller, "1844 - zero-reset heart cam," Zegarki i Pasja, accessed Jun. 06, 2023. [Online]. Available: https://zegarkiipasja.pl/artykul/16788-1844-a-chronograph-reset-hand-return-to-zero

[71] M. Genoud and G. Papi, "Chronograph mechanism and timepiece comprising the chronograph mechanism," May 24 2016, uS Patent 9,348,319.

[72] R. Meis, "Chronograph," Apr. 30 2013, uS Patent 8,432,772.

[73] A. Kruttli and D. Chabloz, "Device for a timepiece," Dec. 3 2019, uS Patent 10,496,039.

[74] W. Reviews, "Iwc gst rattrapante chronograph iw3715-13 iwc watch review," Youtube, accessed Jun. 06, 2023. [Online]. Available: https://youtu.be/QOWYQindqcg?t=206

[75] G. Oster, "The science of moiré patterns," *(No Title)*, 1969.

[76] A. Materials, "1 x 1 x 1mm thick block magnets — c0010," ALB Materials, accessed Jun. 06, 2023. [Online]. Available: https://www.albmagnets.com/block-magnets/3356-neodymium-block-magnets-c0010.html

[77] W. Yang, "Magnetic levitation force exerted on the cylindrical magnet in a ferrofluid damper," *Journal of Vibration and Control*, vol. 23, no. 14, pp. 2345–2354, 2017.

[78] D. K. P. Art, "Learn origami 03 — basic paper fold herringbone tessellation — centripetal & centrifugal grid," Youtube, accessed Nov. 17, 2022. [Online]. Available: https://www.youtube.com/watch?v=R0puJOFnEVw

[79] G. I., "Paper review #12: Kami," Origami USA, accessed Jun. 06, 2023. [Online]. Available: https://origamiusa.org/thefold/article/paper-review-12-kami

[80] T. L. Chow, *Introduction to electromagnetic theory: a modern perspective*. Jones & Bartlett Learning, 2006.

[81] D. J. Griffiths, "Introduction to electrodynamics," 2005.

[82] P. Baillio, "Jewel bearings solve light load problems," *Machine Design*, pp. 111–114, 1989.

[83] Vedantu, "Q&a magnetism," Vendatu, accessed Jun. 06, 2023. [Online]. Available: https://www.vedantu.com/question-answer/a-compass-needle-whose-magnetic-moment-is-60am2-class-12-physics-cbse-5f518ffbc916425872505dfa

[84] M. Tilli, M. Paulasto-Krockel, M. Petzold, H. Theuss, T. Motooka, and V. Lindroos, *Handbook of silicon based MEMS materials and technologies*. Elsevier, 2020.

[85] K. E. Petersen, "Silicon as a mechanical material," *Proceedings of the IEEE*, vol. 70, no. 5, pp. 420–457, 1982.

[86] N. Staff, "Claire & john bertucci nanotechnology laboratory," Carnegie Mellon University, accessed Jun. 06, 2023. [Online]. Available: https://nanofab.ece.cmu.edu/facilities-equipment/asml-wafer-stepper.html

[87] M. K. Emsley, O. Dosunmu, and M. Unlu, "Silicon substrates with buried distributed bragg reflectors for resonant cavity-

enhanced optoelectronics," *IEEE Journal of Selected Topics in Quantum Electronics*, vol. 8, no. 4, pp. 948–955, 2002.

[88] Okmetic, "C-soi® wafers – cavity soi," Okmetic, accessed Jun. 06, 2023. [Online]. Available: https://www.okmetic.com/silicon-wafers/soi-wafers-silicon-on-insulator-line/c-soi-wafers-cavity-soi/

[89] T. Mizuno and T. Kamae, "Mechanical strength of silicon wafers," *Department of Physics, Hiroshima University*, 2000.

[90] S. Wafer, "Silicon wafers," Siegert Wafer, accessed Jun. 06, 2023. [Online]. Available: https://www.siegertwafer.com/datenbankaufruf_silicon.php?s=CO14018

[91] M. A. Hopcroft, W. D. Nix, and T. W. Kenny, "What is the young's modulus of silicon?" *Journal of microelectromechanical systems*, vol. 19, no. 2, pp. 229–238, 2010.

[92] U. Wafer, "What are the mechanical properties of monocrystalline silicon?" University Wafer, accessed Jun. 06, 2023. [Online]. Available: https://www.universitywafer.com/mechanical-properties-monocrystalline-silicon.html

[93] F. Ericson and J.-Å. Schweitz, "Micromechanical fracture strength of silicon," *Journal of Applied Physics*, vol. 68, no. 11, pp. 5840–5844, 1990.

[94] I. M. Lab, "Silicon dioxide/nitride color vs. film thickness and viewing angle calculator," Brigham Young University, accessed Jun. 06, 2023. [Online]. Available: https://cleanroom.byu.edu/color_chart

[95] J. Henrie, S. Kellis, S. M. Schultz, and A. Hawkins, "Electronic color charts for dielectric films on silicon," *Optics express*, vol. 12, no. 7, pp. 1464–1469, 2004.

[96] H. Zhitao, C. Jinkui, M. Fantao, and J. Rencheng, "Design and simulation of blue/violet sensitive photodetectors in silicon-on-insulator," *Journal of Semiconductors*, vol. 30, no. 10, p. 104008, 2009.

[97] F. Ma and G. Chen, "Modeling large planar deflections of flexible beams in compliant mechanisms using chained beam-constraint-model," *Journal of Mechanisms and Robotics*, vol. 8, no. 2, p. 021018, 2016.

[98] J. B. Hopkins and M. L. Culpepper, "Synthesis of multi-degree of freedom, parallel flexure system concepts via freedom and constraint topology (fact)–part i: Principles," *Precision Engineering*, vol. 34, no. 2, pp. 259–270, 2010.

[99] O. with Jo Nakashima, "Origami magic ball (dragon's egg by yuri shumakov)," Youtube, accessed Nov. 17, 2022. [Online]. Available: https://www.youtube.com/watch?v=VgXwSdJNks8

[100] L. Oberson, "Moiré-effect winding assembly for automatic timepiece movement," Jul. 13 2021, uS Patent 11,061,371.

[101] J. D. McGarvey, "Rotational moire timepiece," Dec. 17 1996, uS Patent 5,586,089.

A Visual Effect Collage

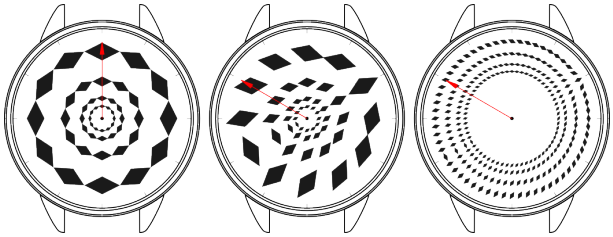

Figure 57: Aiming Diamonds: aiming diamonds at a point where the needle tip would be using the gradient.

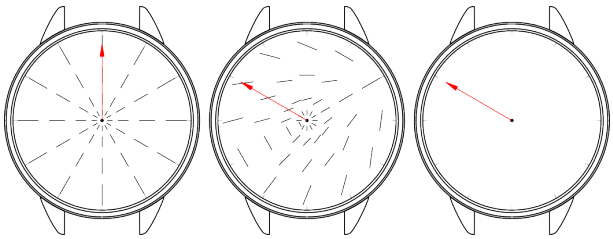

Figure 58: Aiming Lines: aiming lines instead of diamonds at a point where the needle tip would be using the gradient.

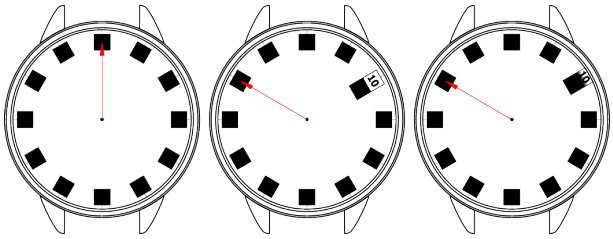

Figure 59: Digital Aperture: by either (2) drawing back a cover or (3) rotating a cube a digital number is brought into view.

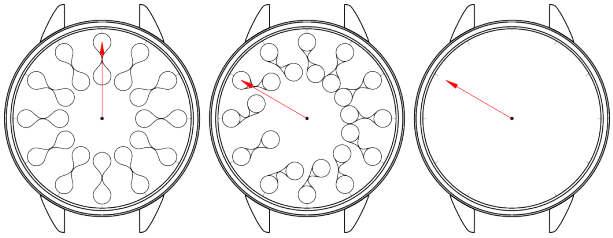

Figure 60: Bending Datawaves: by bending this 'double droplet' towards the indicated second one can see the time.

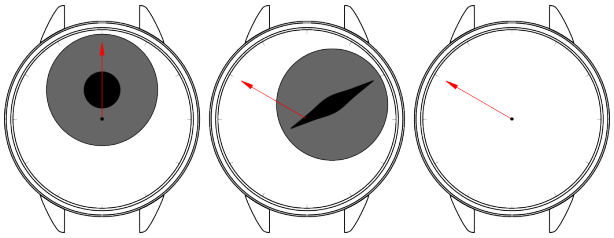

Figure 61: Cat Eye: by changing a human round eye into a cat eye slit it can indicate the time (a bio-inspired idea).

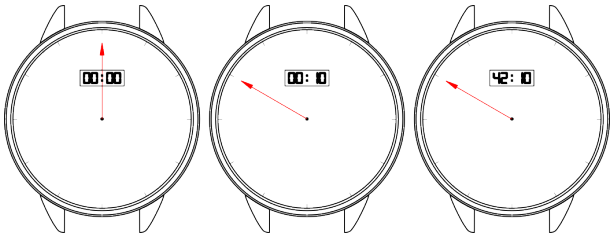

Figure 62: Digital Memory: A digital clock that only displays the time when asked and does not count along with the chronograph.

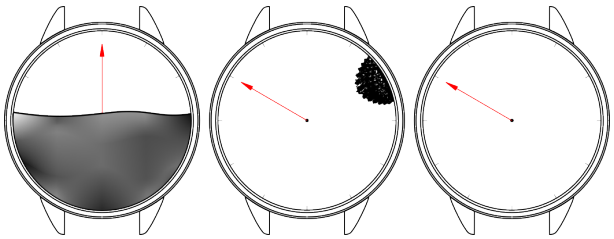

Figure 63: Ferrofluid Loose: by activating a magnet the fluid can center itself around the desired point.

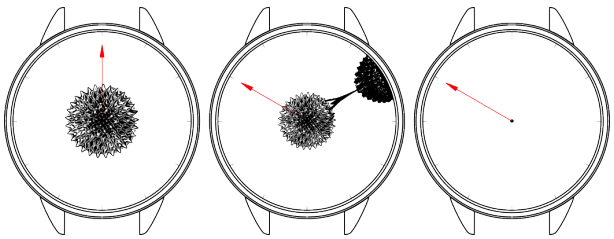

Figure 64

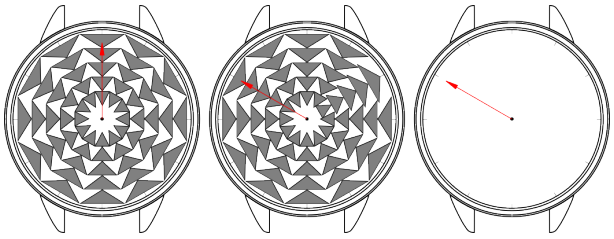

Figure 65: Flipping Triangles: the triangles are flipped over their radial axis to pint at the time.

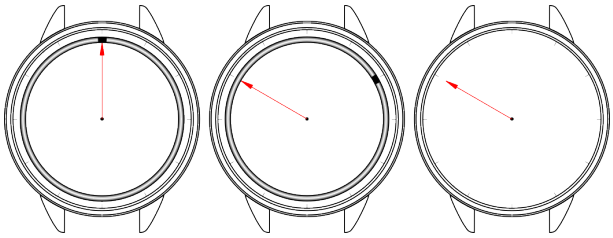

Figure 66: Ferrofluid Tube: a (magnetized) fluid that runs in a tube around the edge.

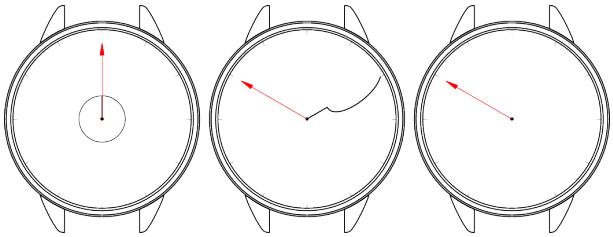

Figure 67: Center Circle Fold-Out: the center circle works a bit like clap bracelets. When released it will bend into the shape shown to indicate the time.

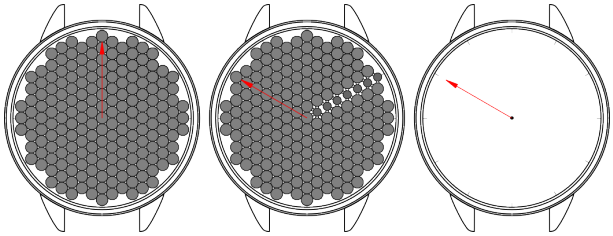

Figure 68: Hexagon Up-Down: the hexagon filled dial can lower a line of hexagon toward the indicated time.

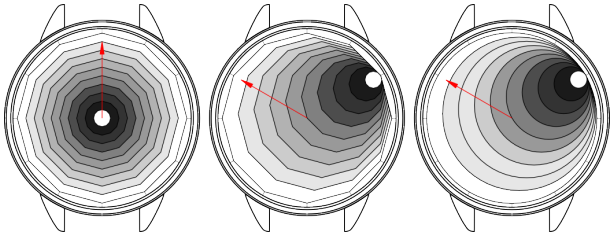

Figure 69: Hexagon Sideways: the hexagonal rings can be actuated toward indicated time. (3) Shows a 60-sides polygon (almost a circle).

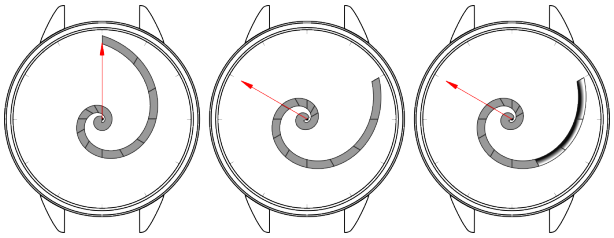

Figure 70: Golden Ratio: the needle is converted to a golden ratio shaped indicator which can, as shown in (3), rotate pieces on the needle to indicate minutes as well as seconds.

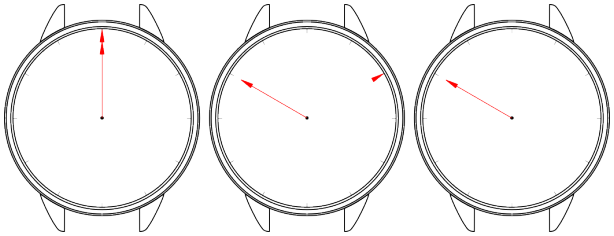

Figure 71: Outer Boundary: the needle arm is removed and the point runs along the outer edge of the dial.

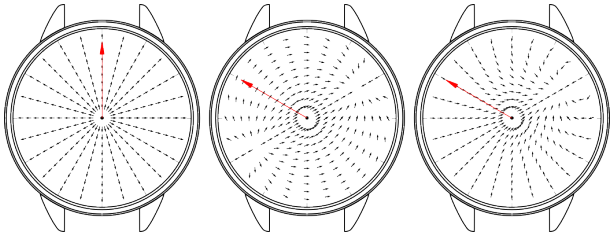

Figure 72: Magnetic Field: by rotating a magnet many compass needles indicate the time along the magnetic field lines.

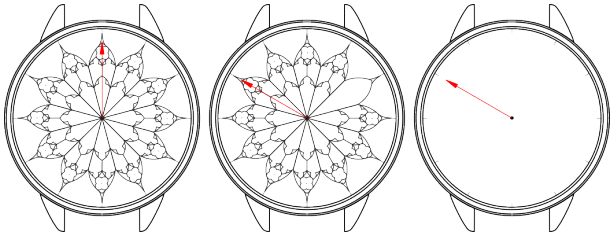

Figure 73: Mandela: by removing the inside pattern of a segment the time is indicated.

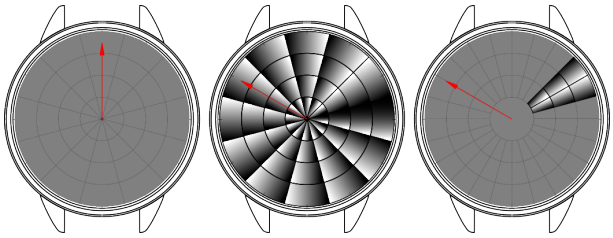

Figure 74: Mechanical Mirrors: by rotating reflective pieces of material, the change in reflection shows the indicated time.

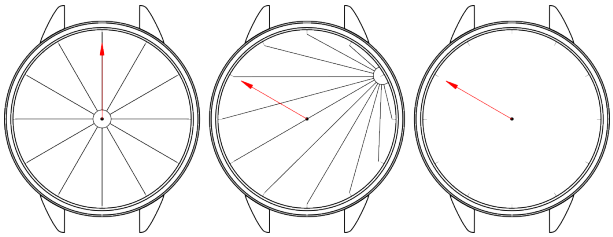

Figure 75: Moving Web: the center of the web is displaced to the outer edge of the watch dial with all the web lines connected to it.

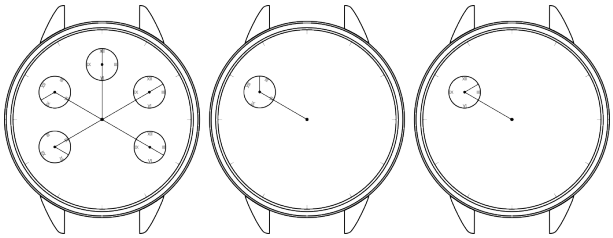

Figure 76: Non-Centric: An extra watch dial is added to the chronograph needle. (2) When stopped the watch dial will keep rotating, such that 50s on the main watch and 50s on the extra dial align. (3) When stopped the needle is stopped and the extra dial will stay in the normal orientation.

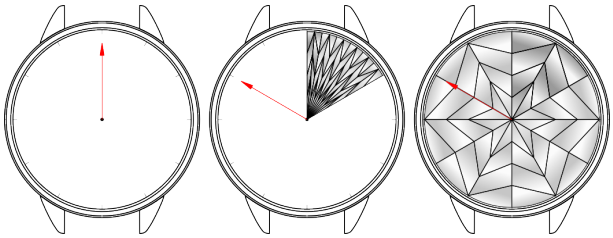

Figure 77: Origami Fan: a 'fan' that can fold out by means of a radial herringbone tessalation to indicate the time.

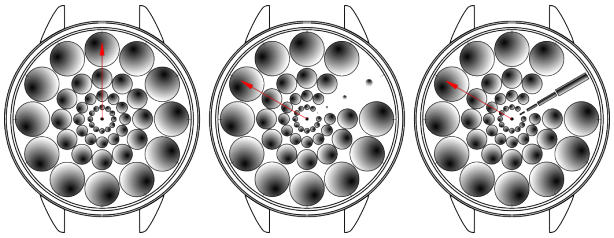

Figure 78: Origami Magic ball: these origami balls can become rods. (2) either in upward facing or (3) radial direction [99].

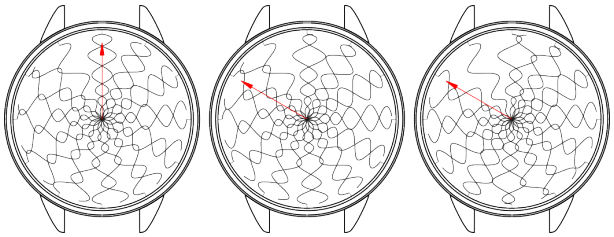

Figure 79: Radial Curves: The lower pattern is stationary and the upper pattern is rotating. The lower pattern is spaced to 360 ° and the upper pattern is spaced to (2) 324 ° or (3) 288 ° to always align the tips of the two patterns at the indicated second.

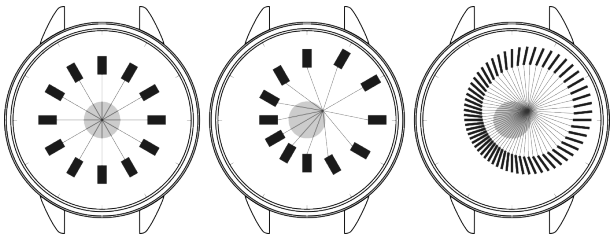

Figure 80: Radial Engine: based on a planes radial engine the pistons move based on the crank position.

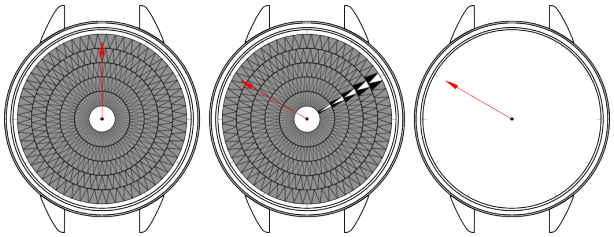

Figure 81: Revolving Pyramids: three radial lines of pyramids are revolved to show another color and indicate the time.

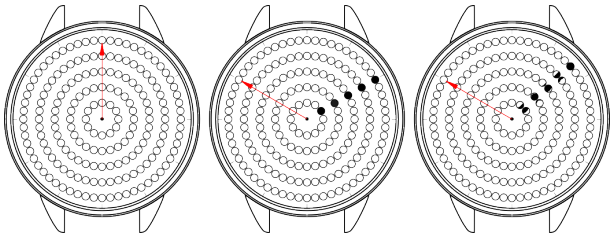

Figure 82: Revolving Spheres: are radial line of two-sides colored spheres are revolved to indicate the time in black and white.

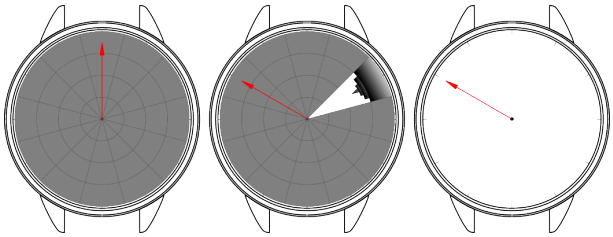

Figure 83: Roof Tiles: based on the tiles of a roof which can retract below each other.

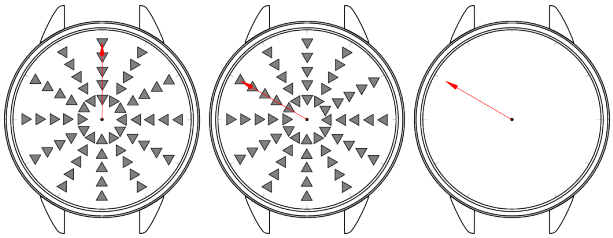

Figure 84: Rotating Triangles: triangles rotate around the normal axis to the dial plane to aim at the desired point.

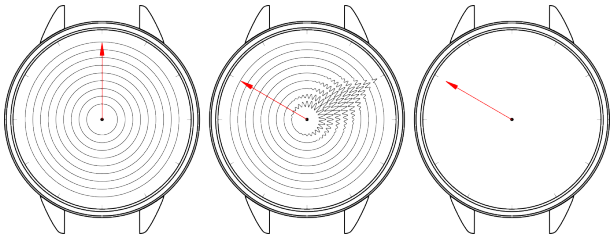

Figure 85: Sine on Circle: by adding sines on different circles the top of the sine create a pointing stucture.

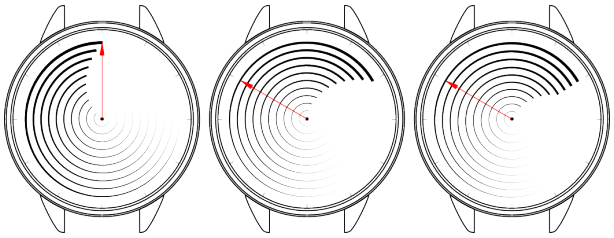

Figure 86: Strokes Align: the strokes rotate along with the chronograph and (2) can be stopped. (3) By aligning the other spirals to the outer one multiple minutes can be indicated.

B Aesthetic Notes

Notes from conversations about the effects not clear from the table

- Sine on circle: Overall lovely effect.
- Ferro Tube: Overall nice effect.
- Origami Fan: Overall nice effect.
- Mech Mirror: The second one is unclear, the third is way clearer, this influenced some opinions and in hindsight it might have been better to not include the second.
- Ferrofluid: Nice effect, even tho an electromagnet might not be achieveable. It might be a bit slow moving and not very precise.
- Spirals: Nice effect, but not everyone found it clear.
- Magnetic Field: Not everyone found it clearly readable. Most people thought the 'Aiming Diamonds' was more clear due to the size of the needles. The effect itself received positive sentiment.
- Aiming Diamonds: The diamond shape was a bit to 'childish' but the effect itself as very clear and nice.
- Revolving Balls: The color on this one made it clear, but some people thought it to busy and the precision (3rd case) for aiming at 8 seconds is not good, The effect would thus need 60 balls per ring.
- Web Moving: People found it more clear than the 'Hex Sideways' but less pretty.
- Outer Edge Indicator: People liked the simplicity of this one, but it does not seem very different than a needle.
- Noncentric: This effect required some explanation since the drawing is quite difficult. Most people liked the idea but questioned the feasibility.
- Revolving pyramids: People were divided over the pretty, It is a clear indication method but to busy in the eyes of some.
- Hex Sideway: People thought this effect was prettier than the 'Web Moving' but less clear.
- Cat eye: Seems closely related to 'Hex Sideway' and 'Moving Web'. This one less pretty and less clear and has less wow-factor.
- Ferro Loose: The 'Ferrofluid' is a much better idea.
- Roof Tiles: The 'Mechanical mirrors' is a much better idea.
- Hex updown: Not clear enough
- Radial Engine: Not clear enough
- Digital aperture: Some really liked this but in the eyes of the invested group it was to much related to a digital watch whereas mechanical watches should stand out from them.
- Golden Ratio: Not clear due to the curve.
- Flipping Triangles: Not clear at all. Maybe color might change that, but still to busy according to most.
- Origami Sphere: To childish according to most

- Bending Datawaves: Nice compliant idea, not clear, more clear if inverted but still not pretty.
- Opening Circle: Unclear idea, not clear and not pretty
- Digital: Same point as 'Digital Aperture'. To much relation to digital watches.
- Radial Effect: Very unclear and therefore to busy and not pretty
- Mandela: Some liked it but most thought it to much work to find the removed piece of the effect.
- Triangles Rotate: Very unclear, color is impossible to achieve in this format.

C Weighting Score Elaboration

A small elaboration of all the scores in Table 4 is given for the reader.

- Moire Sines:
  Friction: 3; Is designed at the limit, so little to no deviation possible. Accuracy: 3; A very small misalignment might give a big inaccuracy. Novelty: 1; Moire has been patented before in [100] and [101]. Visibility: 3; A moire effect is simply not the most clearly visible. Gravity: 5; it is a rigid plate . Assembly: 5; Just a difficult as a needle. Minus: -. Aesthetics: 16.
- Separated Sines:
  Friction: 4; Some wiggle room for structural rigidity. Accuracy: 5; It has frequency of watch and points neatly at specific time. Novelty: 3; It seems quite close to an oversized needle. Also it has no dynamic transition whatsoever. Visibility: 5: It aims directly and according to the survey this effect was very clear. Gravity: 5; Should not have an influence. Assembly: 4; Can be very fragile which requires great care, but it is only one piece. Minus: -. Aesthetics: 16.
- Flipping Sines:
  Friction: 5; Actuated by a vertical clutch. Accuracy: 4; Novelty: 5; Very novel and probably gives a wow factor from different perspectives. Visibility: 4: Parts are quite small, and perpendicular sines might block the view from some angles. Gravity: 4; The sines might be able to flip if not constrained correctly. Assembly: 2; The devised assembly plan (rack, sines, rack) is not easy and very fragile. Minus: -. Aesthetics: 16.
- Ferrofluid in a Tube:
  Friction: 4; The magnet is at is outer point, But the magnetic force is big enough to move it to make way for unaccounted forces so far. Accuracy: 2; The magnetic force becomes 0 when aligned thus it will never be exactly aligned. Novelty: 4; Might resemble [30] a bit, but it is definitely different due to magnetism and the absence of fluid pumps. Visibility: 5; It has great contrast and the fluid is small. Gravity: 4; In upright gravity will pull down the fluid slightly. Assembly: 2; Will be a difficult process due to fluids in watches. Minus: -3; The fact that the return time will be slow is a negative. Aesthetics: 15.
- Mechanical Mirrors:
  Friction: 5; Actuated by a vertical clutch. Accuracy: 4; Exactly 1 second precision. Novelty: 5; It is not seen before in a watch dial. Visibility: 5; Reflection will create a great contrast. Gravity: 5; Should have no influence if the mirrors are compliant or bi-stable. Assembly: 3; Might have to be done in quarter circles, it is very precise, but not fragile. Minus: -. Aesthetics: 11.
- Magnetic Field:
  Friction: 2; Especially if gravitational moments introduce extra friction it might quickly overshoot the friction limit. Accuracy: 1; Might be quite hard to see, especially for people less familiar with magnetic fields and their field lines. Novelty: 5; Still seems amazing. Visibility: 4; Needles with colors will give good contrast. Gravity: 3; It will stay rigid, but might rotate with more friction. Assembly: 1; Assembling over 200 needles through a ruby hole is going to be a mess. Minus: -. Aesthetics: 8 + 2; since the effect has been improved with respect to the survey.